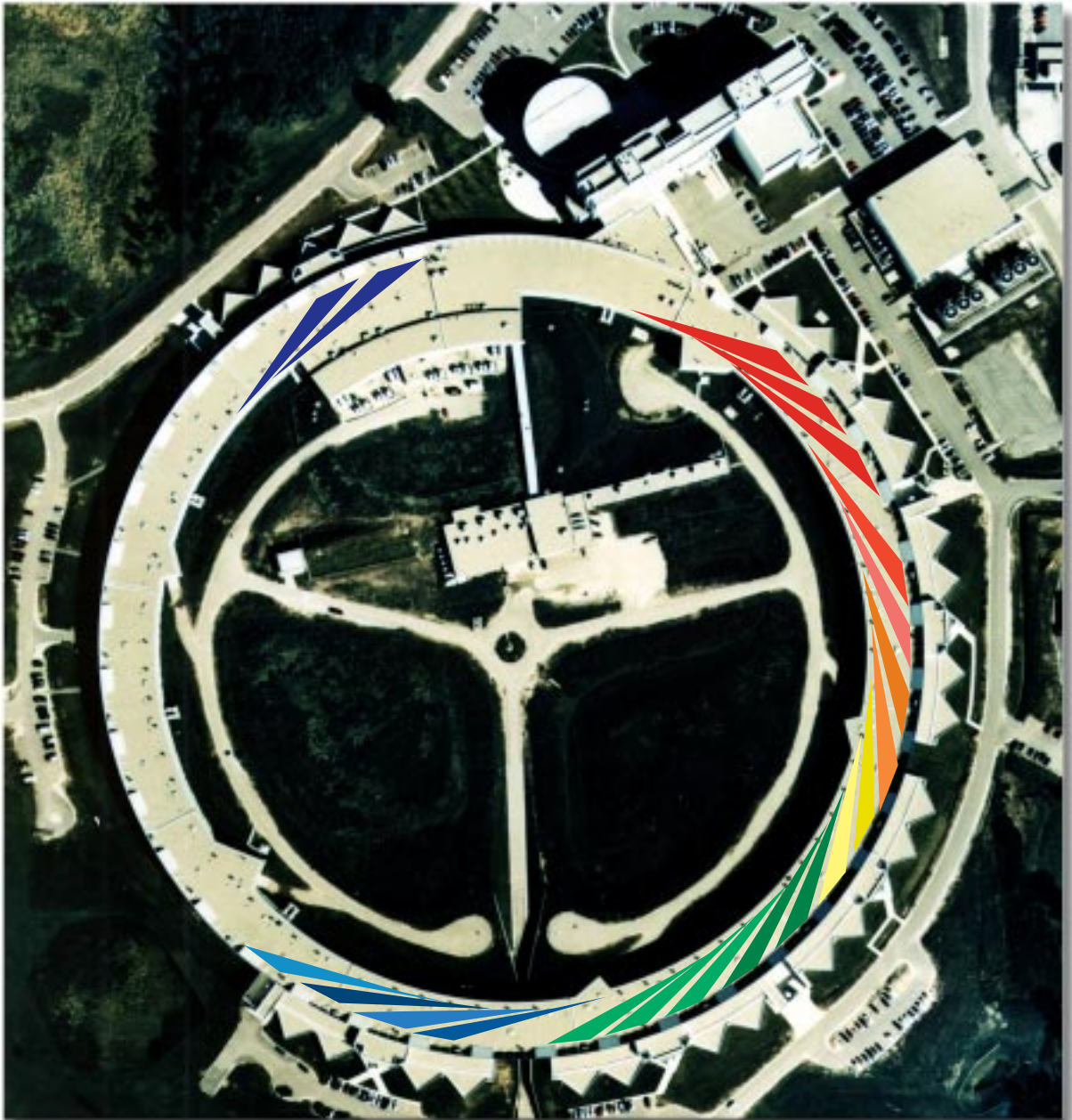


ADVANCED PHOTON SOURCE RESEARCH



VOLUME 1 • NUMBER 1 • APRIL 1998 • ANL/APS/TB-31

ARGONNE NATIONAL LABORATORY IS OPERATED BY THE UNIVERSITY OF CHICAGO FOR THE U.S. DEPARTMENT OF ENERGY
UNDER CONTRACT W-31-109-ENG-38

IN THIS ISSUE



LETTER FROM THE DIRECTOR *DAVID E. MONCTON*

PG. 1



THE ADVANCED PHOTON SOURCE: A BRIEF OVERVIEW

PG. 2



MAD ANALYSIS OF FHIT AT THE STRUCTURAL BIOLOGY CENTER

PG. 6

CHRISTOPHER D. LIMA, KEVIN L. D'AMICO, ISTVAN NADAY, GEROLD ROSENBAUM, EDWIN M. WESTBROOK, & WAYNE A. HENDRICKSON



ADVANCES IN HIGH-ENERGY-RESOLUTION X-RAY SCATTERING AT BEAMLINE 3-ID

PG. 9

ESEN ERCAN ALP, WOLFGANG STURHAHN, THOMAS TOELLNER, PETER LEE, MARKUS SCHWOERER-BÖHNING, MICHAEL HU, PHILIP HESSION, JOHN SUTTER, & PETER ABBAMONTE



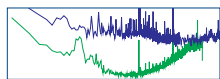
X-RAY IMAGING & MICROSPECTROSCOPY OF THE MYCORRHIZAL

PG. 15

FUNGUS-PLANT SYMBIOSIS *ZHONGHOU CAI, WENBING YUN, STEPHEN T. PRATT,*

RAYMOND M. MILLER, EFIM GLUSKIN, DOUGLAS B. HUNTER, AMIEL G. JARSTFER,

KENNETH M. KEMNER, BARRY LAI, HEUNG-RAE LEE, DANIEL G. LEGNINI, WILLIAM RODRIGUES, & CHRISTOPHER I. SMITH



MEASUREMENT & CONTROL OF PARTICLE-BEAM TRAJECTORIES IN THE ADVANCED PHOTON SOURCE STORAGE RING *GLENN DECKER*

PG. 21



BEAM ACCELERATION & STORAGE AT THE ADVANCED PHOTON SOURCE — OPERATIONS REPORT *ROD GERIG*

PG. 26



EXPERIMENTAL FACILITIES OPERATIONS & CURRENT STATUS *ANTANAS RAUCHAS*

PG. 28



RECENT PUBLICATIONS

PG. 30

ON THE FRONT COVER: The colored segments superimposed on an aerial photograph of the Advanced Photon Source facility indicate experiment hall sectors currently occupied by Collaborative Access Teams. See the back cover of this issue for a description of each team's proposed research initiatives. *(Photograph by the Sidwell Company)*

The Advanced Photon Source is funded by the U.S. Department of Energy, Office of Energy Research, Office of Basic Energy Sciences.

DISTRIBUTION CATEGORY: ATOMIC, MOLECULAR, AND CHEMICAL PHYSICS (UC-411)

This document was prepared as an account of work sponsored by an agency of the United States Government. Neither the United States Government nor any agency thereof, nor any of their employees, makes any warranty, express or implied, or assumes any legal liability or responsibility for the accuracy, completeness, or usefulness of any information, apparatus, product, or process disclosed, or represents that its use would not infringe privately owned rights. Reference herein to any specific commercial product, process, or service by trade name, trademark, manufacturer, or otherwise, does not necessarily constitute or imply its endorsement, recommendation, or favoring by the United States Government or any agency thereof. The views and opinions of authors expressed herein do not necessarily state or reflect those of the United States Government or any agency thereof.

LETTER FROM THE DIRECTOR



Fourteen years ago, the synchrotron research community, at the behest of the Department of Energy (DOE) and the National Research Council, made what proved to be a persuasive case for new, undulator-based, high-brilliance synchrotron x-ray facilities to be used for the study of materials. This came at a time when a greater understanding of the unique capabilities of synchrotron radiation made it the ideal tool for investigating the structure, and thereby elucidating the function, of increasingly complex materials upon which man's technology and nature's biology are founded.

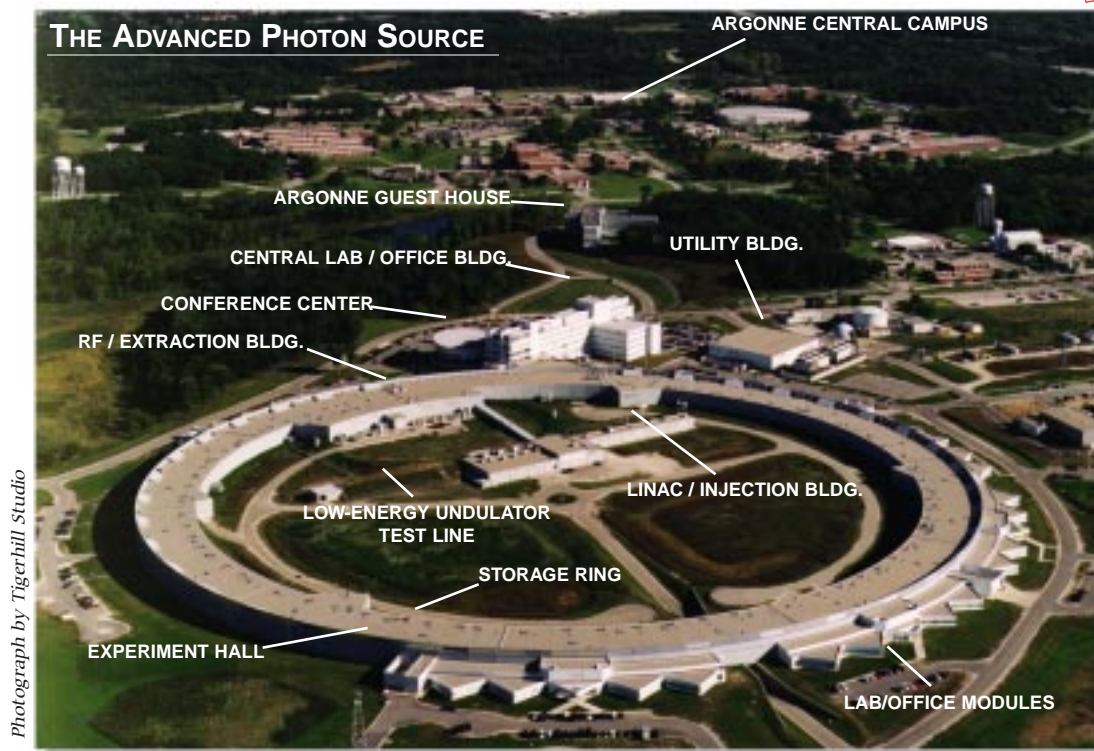
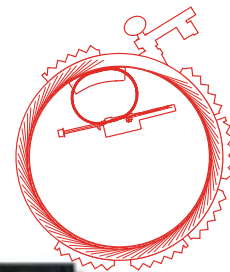
Eleven years after these prescient reports were issued, the Advanced Photon Source (APS) generated its first x-ray beams during the centennial year celebrating Röntgen's great discovery. Now, in 1998, the APS is proving to be an extremely reliable source of x-ray beams for a strong and committed user community. As APS research beamlines begin to take data, there is a growing appreciation for science. Here in Illinois, the State has shown its faith in the promise of the APS by underwriting construction of the Argonne Guest House, a residence for visiting scientists; and providing support for Illinois institutions developing beamlines at the APS.

The federal government is responding to the technological and economic challenges facing the U.S. in part by evaluating the current level of science funding. The Basic Energy Sciences Advisory Committee Panel on DOE Synchrotron Radiation Sources and Science, chaired by Robert Birgeneau, of the Massachusetts Institute of Technology, and vice-chaired by Zhi-Xun Shen, of Stanford University, has recently issued its report, which explores "the nature and scientific importance of synchrotron radiation research, past, present, and future." All of us can be heartened by the committee's conclusion that the field "has evolved from an esoteric endeavor practiced by a small number of scientists...to a mainstream activity, which provides essential information in the materials and chemical sciences, the life sciences, molecular environmental science, the geosciences, nascent technology and defense-related research among other fields."

The Administration and Congress have already begun to act on the committee's funding recommendations for synchrotron-based research, a positive comment on both the committee's work and the field's health. In this promising environment, we offer the first issue of *Advanced Photon Source Research*, a periodical that will highlight some of the results of our users' investigations. The work of those who design, develop, and maintain our technical components will also be reported. We intend this periodical to be another example of the close cooperation between the APS and its users, which I believe has been unique in the history of synchrotron radiation research.

David E. Moncton
Associate Laboratory Director
Advanced Photon Source

THE ADVANCED PHOTON SOURCE FACILITY: A BRIEF INTRODUCTION



The Advanced Photon Source (APS) facility (above) at Argonne National Laboratory is a synchrotron light source funded by the U.S. Department of Energy, Energy Research Division, Office of Basic Energy Sciences. The APS provides insertion device- (ID) and bending magnet- (BM) based synchrotron x-ray radiation for use in front scientific and technological research. Synchrotron radiation is produced by the precision, controlled motion of a low-emittance, high-energy particle beam that is generated and stored by the accelerator system. X-ray beams produced by IDs and BMs are transported via beamlines to research stations, where materials under study are illuminated (Fig. 1). Responsibility for overall APS operations falls on two divisions. The Accelerator Systems Division operates all particle-beam acceleration and storage technical components. The Experimental Facilities Division operates all technical components that deliver x-ray beams to user beamlines, and provides administrative and technical interface with users. The users, as members of Collaborative Access Teams (CATs), finance, manage, and operate their beamlines. Other users not affiliated with CATs gain access to beam time as independent investigators.

PARTICLE-BEAM ACCELERATION & STORAGE

Production of APS x-ray beams begins at the electron gun, a cathode-ray tube, which emits electrons that exit the gun at 100 keV. Thirty-nsec-long pulses of electrons are raised to an energy of 200 MeV at 48 pps by a series of accelerating structures in the first-stage (electron) linear accelerator, or linac. When the 480 W beam of electrons strikes a 7-mm-thick, water-cooled tungsten disk — the positron conversion target — the interaction creates photons, which produce electron-positron pairs. The

APS can operate using either electrons or positrons. In normal operating mode, the second-stage linac, which functions in essentially the same way as the first-stage linac, is phased to optimize positrons, which are accelerated to 450 MeV. Operation with positrons is preferred because their charge repels residual gas ions that might otherwise lead to instabilities that could cause beam loss.

The positron accumulator ring (PAR) collects electrons or positrons from the 60-Hz linac during each cycle of the 2-Hz synchrotron. The PAR is 31 m

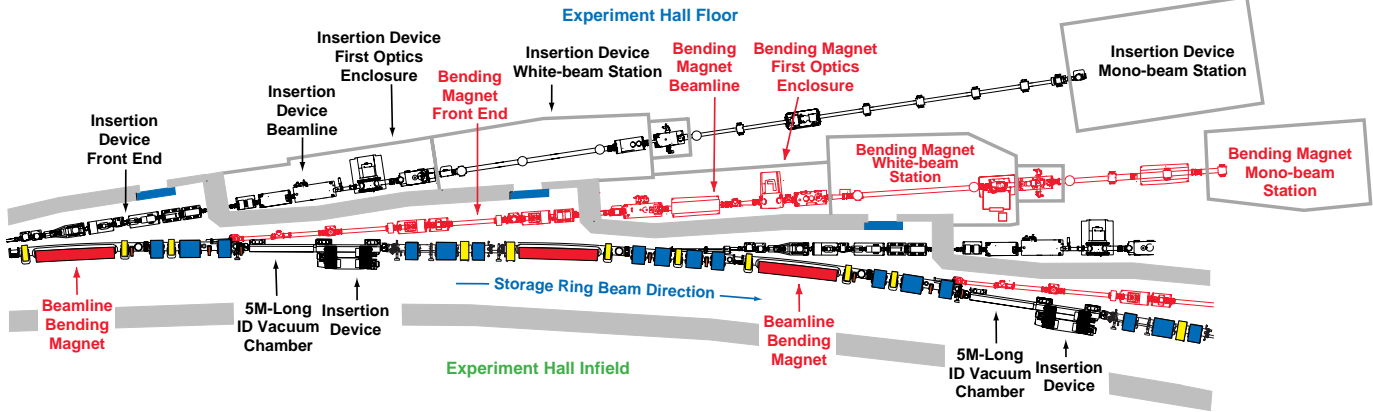


FIG. 1. Diagram of a typical sector at the APS, including storage ring and beamlines.

in circumference. Major magnets are arranged in mirror symmetry along north-south and east-west center lines. Ten to 12 pulses of 450-MeV positrons are collected in 0.55 sec by the PAR and injected as one group into the booster synchrotron.

A 368-m-long, racetrack-shaped booster synchrotron raises positron energies at a rate of 32 keV per turn. The accelerating force is supplied by electrical fields within radio-frequency (rf) cavities operating at 352 MHz, the same frequency used by the storage ring (SR) rf cavities. In 0.25 sec, positrons orbit the booster 200,000 times as their energy climbs to 7 GeV — approximately the speed of light.

The positrons are then injected into the 1,104-m-circumference SR (Fig.2). This circular chain of 1,097 electromagnets contained within a concrete shielding enclosure lies on the inner perimeter of the experiment hall, an annular structure with an exterior radius of 191.4 m, an inner radius of 164.6 m, and a height of 9.8 m. The particle beam is steered and focused by the electromagnets as it circulates within a closed system of 240 aluminum-alloy vacuum chambers running through the magnet centers. Design vacuum inside these chambers is 10^{-9} Torr with beam present. The beam decelerates at a rate of about 6 MeV per turn as it emits synchrotron radiation. This energy loss is replaced by the 352-MHz rf cavities in the SR. Every 10-20 hours, the SR is refilled with positrons.

The SR magnet lattice is configured to provide 40 periods, with 40 corresponding sectors. A typical SR sector comprises 2 dipole magnets, 10 quadru-



FIG. 2. An APS storage ring sector, looking downstream.

pole magnets, 7 sextupole magnets, 8 corrector magnets, 9 rf beam-position monitors, and 6 extruded aluminum vacuum chambers and associated vacuum pumping equipment, all mounted on girders, five per sector. Girders are aligned in the SR tunnel to a tolerance of ± 0.1 mm. Five of the sectors are taken up with beam-injection and rf equipment. The remaining 35 are equipped to provide ID and BM radiation.

RADIATION SOURCES

The SR incorporates 35 5-m-long straight sections available for installation of IDs. At this time, two types of IDs are used to enhance x-ray production: wigglers, which generate very intense x-ray radiation over a wide and continuous range of energies; and undulators, which yield pseudo-monochromatic x-ray radiation with high brilliance, tunable over a wide energy range. The APS currently has 20 IDs installed on the SR. Sixteen of these are



FIG. 3. The elliptical multipole wiggler installed in the APS storage ring.

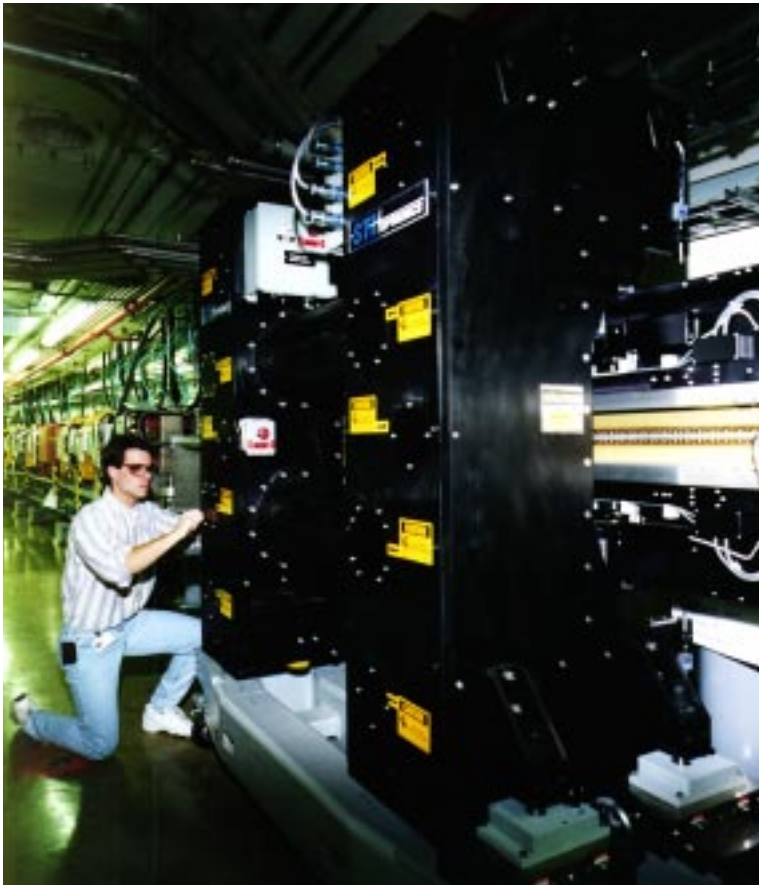


FIG. 4. An undulator A insertion device installed in the APS storage ring.

33-mm-period undulators; two other undulators have periods of 55 mm and 27 mm. The remaining two devices are an 85-mm-period wiggler and a 160-mm-period elliptical multipole wiggler (EMW). The EMW (Fig. 3), built by the APS in collaboration with the Budker Institute of Nuclear Physics in Novosibirsk, Russia, consists of a planar array of permanent magnets and poles to produce a vertical

field component and an electromagnet to generate a horizontal field. The device produces time-varying, circularly polarized x-rays.

The primary ID at the APS is a 2.4-m-long undulator with a 33-mm period (Fig. 4). To achieve the high brilliance and overlapping energy tunability expected from the APS, the undulator design uses wedge-shaped magnetic poles, which increase the effective magnetic field, and a vacuum chamber with very tight tolerances so that the undulator gap can be closed to 10.5 mm. The vacuum chamber maintains these tolerances over a 5-m length and provides an 8-mm aperture for the circulating positron beam. Figure 5 shows a plot of on-axis-brilliance from the APS undulator as a function of energy at the first, third, and fifth harmonics.

The SR lattice also incorporates the necessary beam ports for extracting radiation from 35 of the 80 BMs that maintain the particle beam on an orbital path. Radiation from an APS BM is a white-radiation source with a critical energy of 19.5 keV.

BEAMLINES

The 35 ID and 35 BM beamlines emerge from the SR enclosure as pairs, each pair constituting a sector. The APS can accommodate a total of 70 research beamlines, or 35 sectors.

Radiation is transported from the SR to the research beamlines through beamline front ends (FEs), which are positioned immediately outside the technical components of the SR, but still inside the concrete SR shielding tunnel. The FEs contain safety shutters, photon beam stops, and other components to coarsely define the emerging x-ray beam and, if required, to stop the x-ray beam and provide adequate radiation protection to areas outside the shielding tunnel. Each x-ray source requires an FE, although there are minor differences between the FEs used with an ID and those used with a BM source. Normal incidence heat fluxes in the ID front ends are on the order of 450 W/mm² or higher, and total heat loads approach 10-15 kW.

Funding for the APS included the monies to construct 20 sectors worth of FEs and IDs for user research, and an additional sector for particle-beam diagnostics studies by APS personnel. The remaining 14 IDs and 28 FEs will be built and installed as funding becomes available. At this writing, 20 sectors in the experiment hall are assigned to 14 CATs.

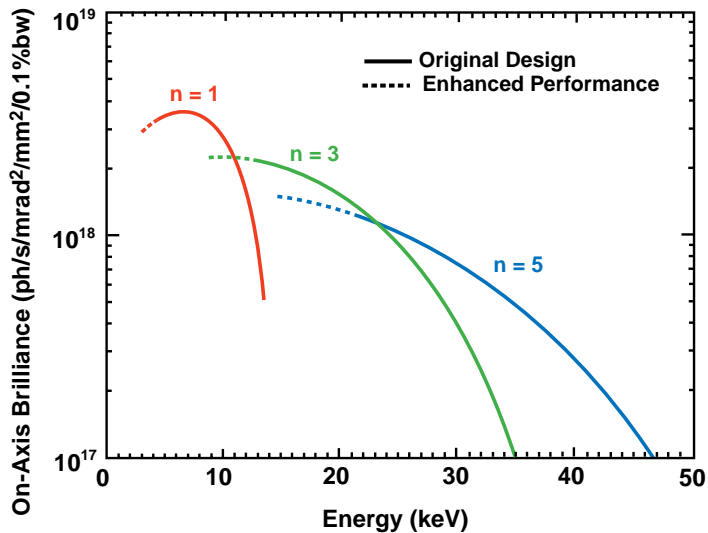


FIG. 5. Tuning curves for the first, third, and fifth harmonics from the 33-mm-period APS undulator (original design vs. enhanced performance).



FIG. 6. Interior of the experiment hall at the sector 1 bending magnet beamline, which is managed by the Synchrotron Radiation Instrumentation Collaborative Access Team.

The research beamlines on the experiment hall floor (Fig. 6) beyond the SR enclosure comprise x-ray optical elements that tailor the beam to support a CAT's scientific goals. These elements are generally contained in the first optics enclosure adjoining the outside of the SR enclosure and include monochromators, filters, and/or mirrors, which are also designed to handle the intense power loads from IDs and to tailor the characteristics of the photon beam to user requirements.

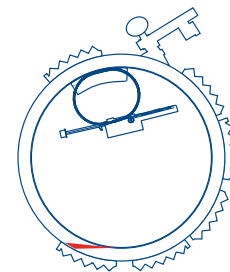
The research stations contain experimental instruments; the sample under investigation; any additional optics needed to analyze and characterize the scattering, absorption, or imaging process; and the detectors. These shielded enclosures also prevent exposure by personnel when the x-ray beam is on. Beam transports, which define and shield the beam path between the various experiment stations, are included as required. Some of the photon beams are split, so that each beamline can have additional branch lines and numerous experiment stations.

COMMISSIONING HISTORY

Commissioning of the APS began with the linac on October 7, 1993. Linac performance requirements with electrons and positrons were met in January and July 1994, respectively, with specified positron current attained in February 1995. Electron beam was first stored in the PAR in mid-April 1994. The first 7-GeV electron beam in the synchrotron booster was produced on January 22, 1995. The first injection of 7-GeV electron beam from booster to SR occurred on February 20, 1995.

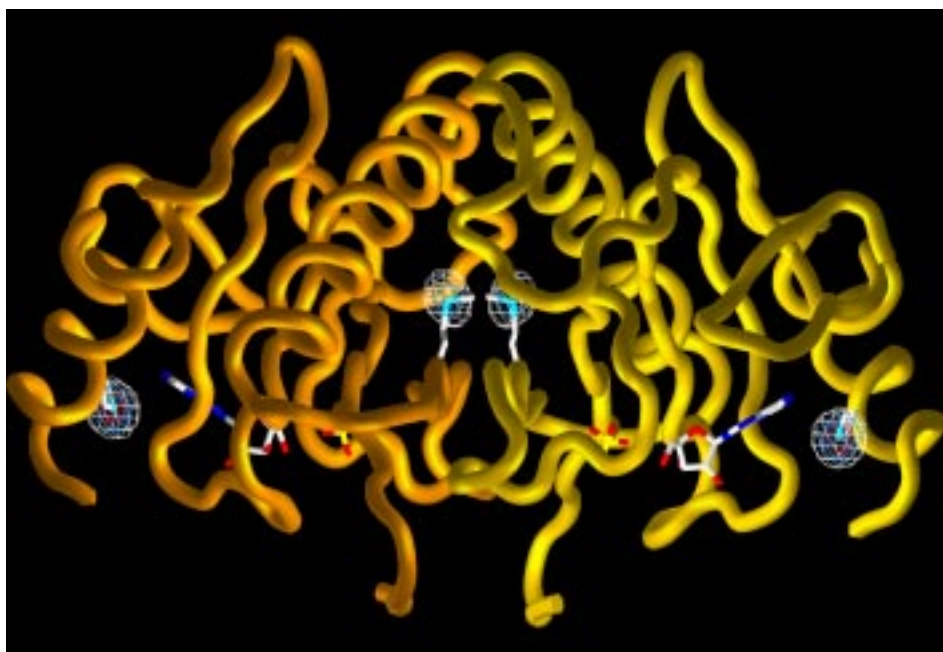
The first turn of 7-GeV electron beam in the SR was achieved on March 18, 1995; a 4.5-GeV electron beam was stored on March 25. On March 26, BM radiation from a stored 4.5-GeV electron beam was detected on the experiment hall floor. Storage of 7-GeV beam occurred on April 16. On July 28, operations with a 12-mm-aperture ID vacuum chamber installed at the sector 1-ID straight section showed no effect on the machine. Shortly thereafter, 8-mA current was stored in a single bunch, well above the design value of 5 mA per bunch. On July 30, 20-mA current was stored in 12 bunches. By August 5, the SR was operating with an undulator in place at the sector 1-ID beamline. On August 9, the first undulator x-ray beam was delivered to the sector 1-ID first optics enclosure. Subsequently, the machine has performed extremely well with two 8-mm-gap ID vacuum chambers in place at sectors 1 and 3. Both chambers have been completely transparent in terms of SR operations. This development bodes well for future operations in that the APS is designed to perform optimally with an 8-mm-aperture vacuum chamber. On October 10, 1995, a new maximum current of 71 mA was attained. On October 11, the machine met the Department of Energy SR commissioning milestone of 20-mA operation and minimum 10 hours of lifetime. ○

MAD ANALYSIS OF FHIT AT THE STRUCTURAL BIOLOGY CENTER*



Christopher D. Lima*, Kevin L. D'Amico[†], Istvan Naday[‡], Gerold Rosenbaum[†],
Edwin M. Westbrook[†], & Wayne A. Hendrickson[§]

*Department of Biochemistry and Molecular Biophysics, Columbia University • [†]Structural Biology Center, Argonne National Laboratory • [‡]Electronics & Computing Technologies Division, Argonne National Laboratory • [§]Howard Hughes Medical Institute, Columbia University



The three-dimensional crystal structure of the putative tumor suppressive fragile histidine triad protein, determined to 1.9-Å resolution by a group using multiwavelength anomalous diffraction data of the selenomethionyl protein (white cages mark four Se sites).

The three-dimensional multiwavelength anomalous diffraction (MAD) structure of the fragile histidine triad (FHIT) protein, a member of a large and highly conserved family of proteins known as the histidine triad (HIT) family of proteins,^{1,2} has been determined by a group using the 19-ID beamline at the Advanced Photon Source (APS). Although their *in vivo* function is still unknown, HIT proteins have been implicated in the binding and hydrolysis of nucleotide polyphosphates. It is likely that such a highly conserved family of enzymes, shown by the high sequence similarity among organisms ranging from mycoplasma, archae, bacteria, plants, and humans, are involved in some critical and ubiquitous biochemical pathway that remains undiscovered, several features of which were later identified by members of the same group (C.D. Lima, M. G. Klein, W.A. Hendrickson, "Structure-based Analysis of Catalysis and Substrate Definition in the HIT Protein Family," *Science* 278, 286-290, [1997]).

*Excerpted from "MAD analysis of FHIT, a putative human tumor suppressor from the HIT protein family," by Christopher D. Lima, Kevin L. D'Amico, Istvan Naday, Gerold Rosenbaum, Edwin M. Westbrook, and Wayne A. Hendrickson, *Structure*, 5, (6), 763774, (June 15, 1997). Reprinted by permission of Current Biology, Ltd.

FHIT, a gene that resides within a fragile site of human chromosome 3, has been postulated to be a human tumor suppressor gene. Unlike the p53 gene, few point mutations have been discovered in the coding regions of the FHIT gene. Instead, disruptions and translocations seem to be the major factors that alter the FHIT translation product. These alterations usually affect only one copy of the FHIT gene in the genome, leaving one full-length copy available in the cell. On the basis of the structure of the FHIT protein, it is unlikely that truncated forms of the protein resulting from altered FHIT transcripts would be capable of folding and interacting with the full-length gene product, thus eliminating the possibility of a dominant negative phenotype when one altered FHIT transcript exists in the cell with one full-length copy of the gene.

This study provides the first structure of FHIT, a diverse member of the HIT family of proteins, and suggests that distant members within the HIT superfamily share a similar overall fold and catalytic mechanism, some features of which can be extended to and inferred from the GalT family of proteins. As the catalytic activity observed *in vitro* demonstrates the ability of these enzymes to hydrolyze their substrates, it is likely that these enzymes could behave as nucleotidyl phosphotransferases through a pathway mediated via a covalent enzyme intermediate — several features of which can be inferred from the FHIT-nucleotide-analog complex. These studies support a mechanism in which the nucleophilic attack by respective histidines in various HIT family members at the α -phosphorus atom would result in a transient covalently attached nucleotidyl-protein intermediate before hydrolysis of the phosphoramidate bond.

EXPERIMENTAL TECHNIQUES

The Structural Biology Center (SBC) beamline 19-ID at the APS utilizes an undulator insertion device to generate very bright x-rays in narrow tunable harmonic peaks. The APS operates at suitably high particle energy to provide the first undulator harmonic in the x-ray range for MAD experiments at the K edge of selenium. The structure of FHIT has been determined by MAD phasing³ using the selenomethionyl protein⁴ in both its free and adenosine/sulfate-bound forms. The data for free and ligand-bound forms of FHIT were measured with the SBC APS1 3x3 charge-coupled device (CCD) array detector⁵ and a FUJI image plate (IP) system, respectively. Both four-wavelength experiments took advantage of the ability to tune the peak of the harmonic by altering the gap width of the undulator during data collection, as has been done previously.⁶ Three gap widths were chosen to center the peak of the first harmonic at the wavelength of choice. A single setting sufficed for peak and inflection points of the selenium K

edge, which are very close together. Both experiments utilized crystals of the selenomethionyl-FHIT protein, although one of the crystals was also soaked in an adenosine/vanadate mixture in order to obtain a complex between protein and nucleoside. The nucleoside soak severely limited the diffraction quality of this sample in comparison with the free form of the protein. Although this enabled two independent structure determinations, it hampered the ability to compare results from the IP system and the CCD detector directly.

An almost complete set of phases was obtained by MADSYS³ analysis to 2.8 Å spacings for the FHIT-adenosine/sulfate complex IP data set. This gave a fully interpretable Fourier map, whereupon the chain was traced and all ordered amino acid residues were positioned. A partially complete phase set was calculated to 2.0 Å spacings for the free FHIT CCD-data set, which resulted in an incomplete and disconnected electron density map. The limited extent of this data set was due to a time constraint, which prevented the completion of the experiment, and to an abundance of saturated low-angle reflections ($d > 5.0$ Å). The addition of phased reflections out to 5.0 Å spacings from the IP data set and density modification⁷ at 2.0 Å yielded readily interpretable maps at 2.0 Å resolution, which allowed the peptide chain to be retraced and sidechains to be positioned.⁸ Although these differences make it difficult to compare the strategies and detectors used in the two experiments, the merging and phasing statistics from both experiments demonstrate that undulator beamline 19-ID and the CCD detector are capable of producing data of sufficient quality for accurate MAD phasing. Ultimately, the native structure was refined against a more complete and higher resolution data set that was measured at beamline X4A at the National Synchrotron Light Source.

DESCRIPTION OF THE FHIT STRUCTURE

The electron density for native FHIT was well-enough defined to complete the model for residues 2-106 and 127-147, but not for the intervening segment or the first residue. Elution of FHIT upon size exclusion chromatography suggests that it is a dimer in solution and, although there is only one chain per asymmetric unit in the crystal, a dimer interaction similar to that previously reported for the PKCI dimer⁹ is observed across a crystallographic twofold axis. The overall structure of the FHIT protomer can be described as a general $\alpha + \beta$ type and further subclassified as an $\alpha + \beta$ meander fold.¹⁰ The FHIT protomer contains two helices, A and B, and seven β strands. Strands 3 to 7 form a five-stranded antiparallel sheet and antiparallel strands 1 and 2 form a β hairpin across from and at an angle to the other sheet. In the protomer, helix A packs on one side of the five-stranded antiparallel sheet. Helix

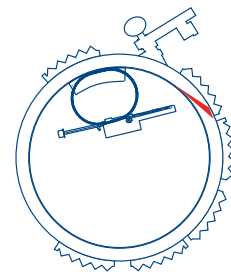
B packs on the same side of the molecule as helix A and primarily interacts with strands 3 and 4 and the loop connecting strands 2 and 3. Two protomers are brought together in the dimer by interactions between helices A and A' and by the formation of a ten-stranded antiparallel sheet comprising the respective five-stranded antiparallel sheet of each protomer. A common hydrophobic core is formed from the protomer interactions within the context of the dimer. The extensive dimer interface occupies 2374 Å² per dimer compared to the total dimer surface area of 11239 Å² as computed with a probe radius of 1.4 Å.¹¹

With the structure of FHIT at hand, the deletion of specific exons from the FHIT locus, which in turn codes for the aberrant FHIT transcripts observed in many cancer cell lines and primary tumors, can be analyzed in terms of protein structure.¹²⁻¹⁶ Several of these aberrant transcripts have been sequenced, and details of the specific deleterious effects on FHIT transcripts have been described. Most of the observed deletions in the FHIT gene either truncate or eliminate the coding regions. Specific exons are deleted in some cases, leading to the possibility of a fused protein. Analysis of any of these deletions mapped onto the three-dimensional structure lead us to believe that none of these mutant proteins would fold and dimerize with the full-length FHIT protein; thus, it is unlikely if not impossible to have a dominant negative phenotype when one copy of the gene is found to be aberrant in length or sequence. This does not exclude the possibility of dose-dependent effects of FHIT expression when one copy of the gene has been disrupted. ○

REFERENCES

- 1 B. Seraphin, The HIT protein family: a new family of proteins present in prokaryotes, yeast and mammals. *J. DNA Seq. Map.* **3**, 177-179 (1992).
- 2 K. Robinson and A. Aitken, Identification of a new protein family which includes bovine protein kinase C inhibitor-1. *Biochem. J.* **304**, 662-664 (1994).
- 3 W. A. Hendrickson, Determination of macromolecular structures from anomalous diffraction of synchrotron radiation. *Science* **254**, 51-58 (1991).
- 4 W. A. Hendrickson, J. R. Horton, and D. M. LeMaster, Selenomethionyl proteins produced for analysis by multiwavelength anomalous diffraction (MAD): a vehicle for direct determination of three-dimensional structure. *EMBO J.* **9**, 1665-1672 (1990).
- 5 E. Westbrook, CCD-based area detectors. *Methods Enzymol.* **276**, 244 (1997).
- 6 L. Shapiro, et al, and W. A. Hendrickson, Structural basis of cell-cell adhesion by cadherins. *Nature* **374**, 327-337 (1995).
- 7 J. P. Abrahams and A. G. W. Leslie, Methods used in the structure determination of bovine mitochondrial F1-ATPase. *Acta Cryst. D* **52**, 30-42 (1996).
- 8 T. A. Jones, J. Y. Zou, S. W. Cowan, and M. Kjeldgaard, Improved methods for building protein models in electron density maps and the location of errors in these models. *Acta Cryst. A* **47**, 110-119 (1991).
- 9 C. D. Lima, M. G. Klein, I. B. Weinstein, and W. A. Hendrickson, Three-dimensional structure of human protein kinase C interacting protein 1, a member of the HIT family of proteins. *Proc. Natl. Acad. Sci. USA* **93**, 5357-5362 (1996).
- 10 C. A. Orengo and J. M. Thornton, Alpha plus beta folds revisited: some favoured motifs. *Structure* **1**, 105-120 (1993).
- 11 A. Nicholls, K. A. Sharp, and B. H. Honig, Protein folding and association: Insights from the interfacial and thermodynamic properties of hydrocarbons. *Prot. Struct. Funct. Genet.* **11**, 281-296 (1991).
- 12 M. Ohta, et al., and K. Huebner, The FHIT gene, spanning chromosome 3p14.2 fragile site and renal carcinoma-associated t(3;8) breakpoint, is abnormal in digestive tract cancers. *Cell* **84**, 587-597 (1996).
- 13 G. Sozi, et al., and C. M. Croce, The FHIT gene at 3p14.2 is abnormal in lung cancer. *Cell* **85**, 17-26 (1996).
- 14 G. Sozzi, et al., and C. M. Croce, Aberrant FHIT transcripts in Merkel cell carcinoma. *Cancer Res.* **56**, 2472-2474 (1996).
- 15 M. Negrini, et al., and C. M. Croce, The FHIT gene at 3p14.2 is abnormal in breast carcinoma. *Cancer Res.* **56**, 3173-3179 (1996).
- 16 L. Virgilio, et al., and C. M. Croce, FHIT gene alterations in head and neck squamous cell carcinomas. *Proc. Natl. Acad. Sci. USA* **93**, 9770-9775 (1996).

ADVANCES IN HIGH-ENERGY-RESOLUTION X-RAY SCATTERING AT BEAMLINE 3-ID



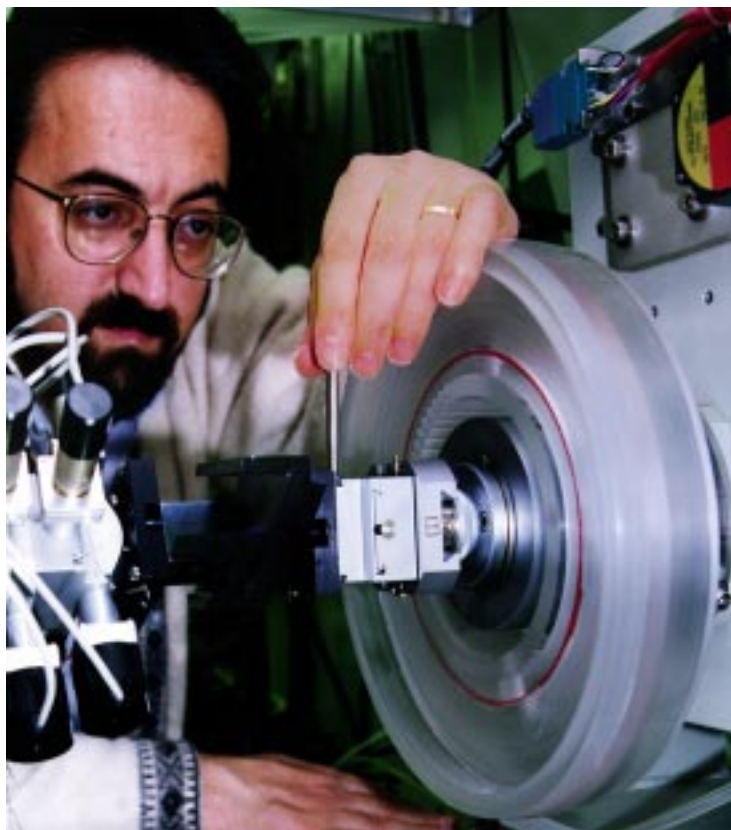
Esen Ercan Alp, Wolfgang Sturhahn, Thomas Toellner, Peter Lee,
Markus Schwoerer-Böhning, Michael Hu, Philip Hession, John Sutter,
& Peter Abbamonte

Experimental Facilities Division, Argonne National Laboratory

Inelastic x-ray scattering is a powerful and important tool for the study of collective excitations in condensed matter systems. The technique measures the dynamic structure factor, which leads to an understanding of electron or atomic correlations in space and time. At moderate energy resolutions (few hundred meV), electron correlations can be studied in metallic systems, strongly correlated electron systems, etc.

At ultra-high energy resolution (a few μeV to meV) the dynamic correlations of ion cores (phonons) can be studied using the inelastic x-ray scattering technique in systems where traditional methods such as neutron scattering may be less applicable. These include ultra-high-resolution nuclear-x-ray-inelastic-scattering to derive partial phonon density of states from disordered systems, thin films, nano-particles, etc. The ultra-high-energy-resolution x-ray experiments will also focus on the dynamics in glasses and liquids.

High-energy-resolution scattering capabilities developed at the Advanced Photon Source (APS) to perform these investigations are the focus of this article, and they directly benefit from the high brilliance of APS undulator sources.



Beamline 3-ID at the APS is one of the strategic instruments used by the Synchrotron Radiation Instrumentation Collaborative Access Team (SRI-CAT). This beamline is dedicated to high-energy-resolution x-ray scattering studies. With optics suitable for $\Delta E/E$ ranging from 10^{-5} to 10^{-13} in the 6-30 keV range, the beamline is equipped with some unique instrumentation developed specifically for the production of x-rays with meV and neV band-pass. Experiments in 1997 have focused on the development of new high-energy-resolution monochromators (shown above) and analyzers based on crystal optics and timing techniques. Applications of

the newly developed techniques include the first sub-meV x-ray spectrometer to record iron phonon density of states in iron metal and in Fe_3Al as a function of order-disorder phase transformation; vibrational dynamics measurements in iron thin films and multilayers and interfaces; observation of partial phonon density of states in Sn and Eu compounds; and measurement of phonon dispersion relations as a function of momentum transferred in diamond and chromium.

The general approach followed when conducting high-energy-resolution experimentation at APS beamline 3-ID was to unify the monochromatiza-

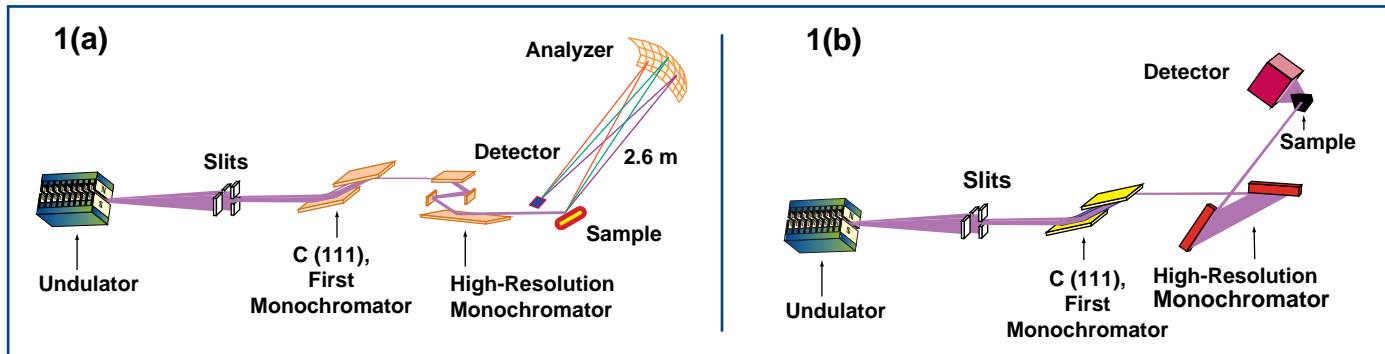


FIG. 1. The schematic layout for high-energy-resolution inelastic x-ray scattering as implemented at the 3-ID beamline of SRI-CAT. 1(a) The inelastic x-ray spectrometer that consists of an “in-line,” nested, 2-channel-cut design high-resolution monochromator followed by a curved crystal analyzer. 1(b) The inelastic nuclear resonant scattering spectrometer that consists of two flat-crystal monochromators followed by a fast detector with nano-second resolution for time discrimination. An in-line monochromator as shown in 1(a) is also available for several isotopes for coherent or incoherent nuclear resonant scattering.

tion process and develop different styles of analyzers. The inelastic x-ray scattering setup using an “in-line” monochromator and curved crystal backscattering is shown in Fig. 1(a), and the configuration for inelastic nuclear resonant scattering is shown in Fig. 1(b).

HIGH-ENERGY-RESOLUTION MONOCHROMATORS

The underlying principle in high-energy-resolution monochromatization is to employ an optimum combination of asymmetrically cut single-crystal reflections to create the desired energy bandpass, angular acceptance, and overall efficiency or throughput. Several different software packages have been developed to optimize certain parameters, such as the choice of reflection planes, the degree of asymmetry, and energy resolution.¹ These programs include calculation of modified DuMond dia-

grams²; accurate three-dimensional (angle-energy-reflectivity) throughput calculations of multiple-crystal systems, including the source divergence and bandpass³; and the complete treatment of multi-beam excitations in single crystals, including exact backscattering.⁴

A summary of crystal monochromators developed is given in Table I. The choice of energy is dictated by specific nuclear resonance or exact backscattering geometry. The nuclear resonance provides a unique way of analyzing energy exchange of photons with phonons by tuning the incident beam energy around the nuclear resonance energy and exciting the resonance via phonon exchange, which then leads to extraction of momentum-integrated partial density of states. The back-scattering geometry, on the other hand, provides the possibility of measuring phonon dispersion relations using single

TABLE I. Crystal monochromators available at the high-energy-resolution beamline 3-ID as of October 1997.

E (keV)	Description	ΔE (meV)	ph/sec/ ΔE /100 mA Measured Flux	Notes
8.4	Si (333) Si (444)	15	N/A	2-nested channel cuts
13.841	Si (422) Si (884)	5.5	5×10^9	2-nested channel cuts
14.413	Si (422) Si (10 6 4)	5.6	1.1×10^{10}	2-nested channel cuts
14.413	Si (975) Si (975)	0.84	6×10^8	2-flat crystal
14.413	Si (975) Si (975)	0.66*	3×10^8	2-flat crystal
21.50	Si (440) Si (15 11 3)	1.0	2×10^8	2-flat crystal
23.880	Si (400) Si (12 12 12)	3.4	8×10^8	2-flat crystal

* The monochromators differ in the asymmetry used in preparing the crystals.

crystals. It is worthwhile to note that the energy bandpass of 0.66 meV at 14.413 keV with 3×10^8 photons/sec represents the highest photon flux with the lowest $\Delta E/E$ achieved so far, using the flat-crystal concept described in^{1,5,6}.

HIGH-ENERGY-RESOLUTION ANALYSIS TECHNIQUES

Analysis of the energy spectrum of inelastically scattered x-rays with sufficient resolution and efficiency continues to be a challenge. The conflicting aspects of this method stem from the divergent nature of the scattered x-rays and the limited angular acceptance of crystals used as analyzers. The problem becomes particularly serious when the required resolution drops below 10 meV in the 6-30 keV range. The established method, originally introduced in the early 1980s,⁷ involves the use of near-backscattering geometry from high-order Bragg reflections. In order to improve the total solid angle subtended by the analyzer, the thin crystal would be bent to a spherical shape with several-meters radius of curvature. This, accompanied by several different procedures to reduce or eliminate bending stress,^{8,9} provides a reasonable solution to an immediate problem.

We have developed a new procedure for use in preparing 10-cm-diameter diced analyzers comprising approximately 8,000 crystals. With respect to earlier methods, we take a new approach to reducing the strain on the curved analyzer. We use a Pyrex wafer as substrate to position the 8,000 crystals. Then, the Pyrex-epoxy-silicon "sandwich" is pressed into a concave substrate with a 2.6-m bending radius.¹⁰

the use of backscattering geometry provides an opportunity to measure phonon frequency-momentum dispersion relations along high-symmetry crystallographic directions from single-crystal samples. Figure 2 shows an example of a phonon dispersion in diamond along the [111] direction. Figure 3 demonstrates the capability for studying phonons in transition metals.

The unique nature of the beamline 3-ID spectrometer lies in the use of a tunable, in-line nested high-resolution monochromator¹¹⁻¹³ to make energy scans instead of the traditional route employing temperature scans of the monochromator or the analyzer. There are several advantages to the in-line geometry. First, there is no need to scan the entire spectrum to find the dispersion of a particular phonon mode as a function of scattering angle, since it achieves energy analysis by tuning the angle of the monochromator crystals with respect to the beam ($0.5 \mu\text{rad}/\text{meV}$ for the inner crystal Si (884) and $0.03 \mu\text{rad}/\text{meV}$ for the outer crystal Si (422)). This saves considerable time in data collection, where one can jump from the elastic peak to the

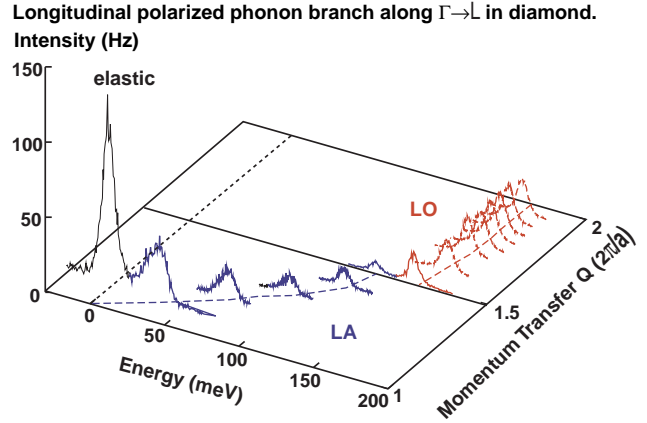


FIG. 2. Spectra at different momentum transfers representing longitudinal acoustic and optic modes in diamond along the [111] direction (L). The measurements were carried out using the Si(777) reflection of the analyzer at a Bragg angle of 89.97° with a total energy resolution of 7.5 meV. These data prove that there is no measurable overbending in the optical mode as predicted by ab-initio calculations.

Longitudinal acoustic phonons along $\Gamma \rightarrow H$ in chromium

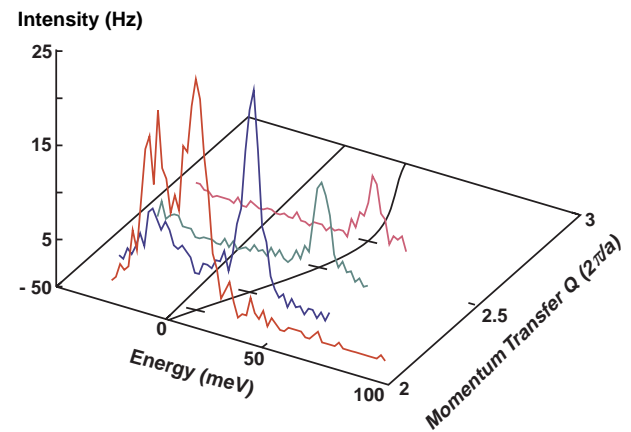


FIG. 3. Studies of phonons in chromium, demonstrating the performance of the instrument for high-resolution inelastic x-ray scattering.

phonon peak directly. The second advantage is the flexibility in beamline optics, which enables this type of scattering study in many beamlines that are suitable for x-ray diffraction. It does not dictate the beamline optics design the way backscattering monochromators would, and it reduces the total length of the beam, minimizing the effects of beam movement. Finally, the in-line monochromators are tunable over several hundred eV, and they form a basis for inelastic scattering studies from other elementary excitations, like plasmons, where the energy resolution can be a fraction of eV, and yet excitations may extend over a larger energy range. *cont'd on page 14*

FIG. 4. Monochromator designs in 3-ID: (a) A nested, 2-channel-cut, high-energy-resolution, high-angular-acceptance monochromator to provide monochromatic x-rays parallel to the incident x-ray beam. The first and last reflection faces are usually of lower order silicon reflections to provide the angular acceptance, while the inner crystal is cut such that higher order reflections provide the desired energy resolution. The angle-energy-reflectivity relation shown on the right-hand side is calculated for Si (422) (10 6 4) reflections at 14.413 keV. (b) Two highly asymmetrically cut silicon crystals optimized to achieve sub-meV energy resolution at an x-ray energy of 14.413 keV. The very high asymmetry angle used for the first reflection results in a grazing angle of 0.46° and consequently is most efficient when used with undulator sources that produce beams of small spatial extent. The measured energy resolution from this design is $660 \mu\text{eV}$ ($\Delta E/E = 4.6 \times 10^{-8}$). A similar concept has been used to achieve 3.4-meV resolution at 23.880 keV, and 1 meV at 21.541 keV. The contour plots on the top correspond to 50% of peak reflectivity.

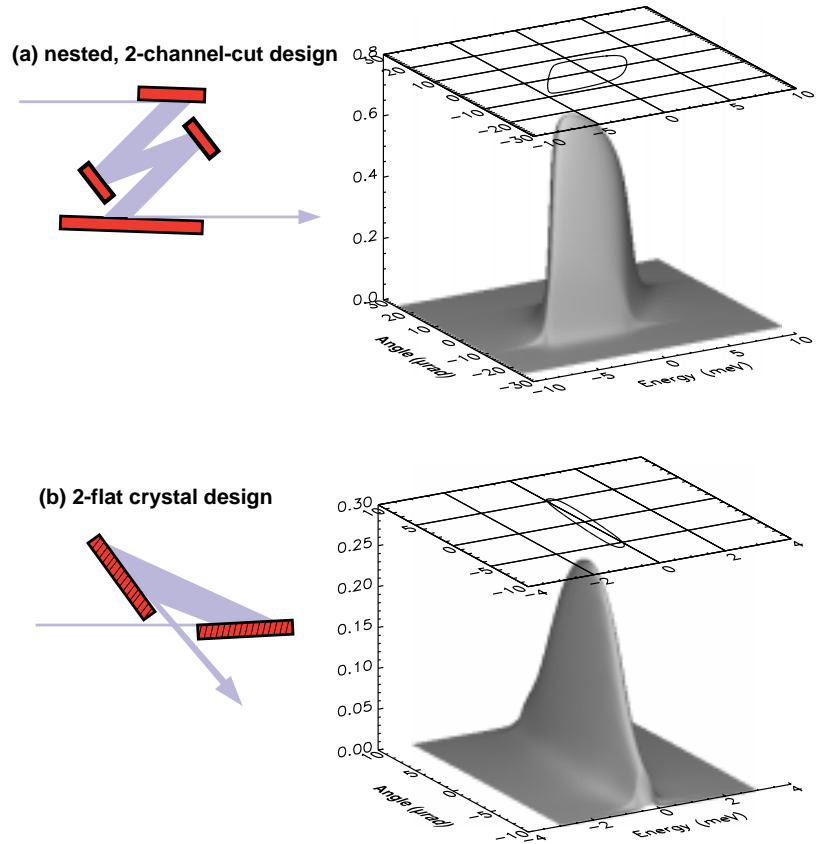
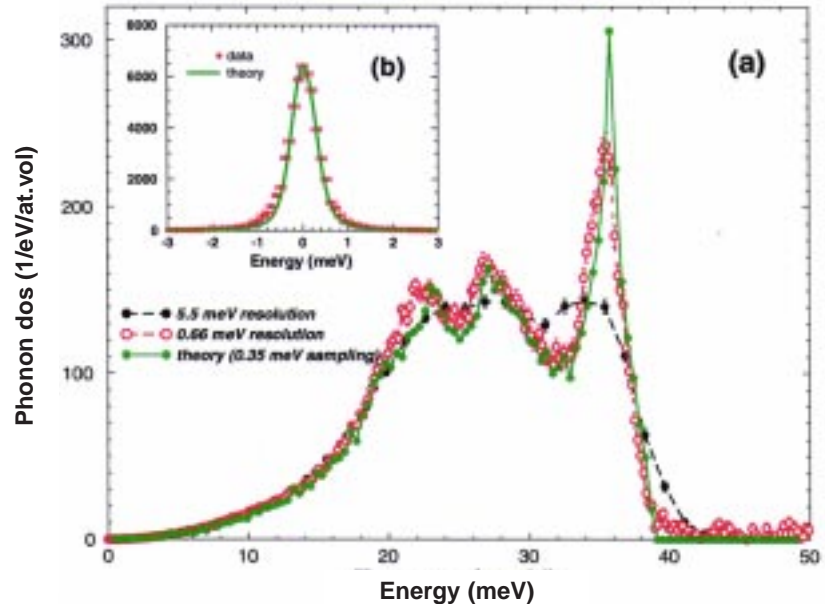


FIG. 5. (a) The phonon density of states of iron measured by inelastic nuclear resonant scattering. The black-filled circles were measured using a 5.5-meV nested monochromator, while the red, empty circles were measured with 0.66-meV resolution, 2-bounce flat crystals. The theory curve is calculated from experimentally determined force constants via fitting the coherent neutron scattering data (courtesy of B. Fultz). (b) The inset shows the resolution function of the 0.66-meV monochromator as measured with coherent nuclear forward scattering. The theoretical calculation includes the brilliance function of the incident beam coupled to the dynamical diffraction equations. The low dispersion points corresponding to higher density of states at 23 and 28 meV are the two transverse acoustical modes, while the peak at 37 meV is the longitudinal acoustic mode. A direct knowledge of phonon density of states is essential in the calculation of classical thermodynamic quantities like heat capacity, entropy, and thermal conductivity.



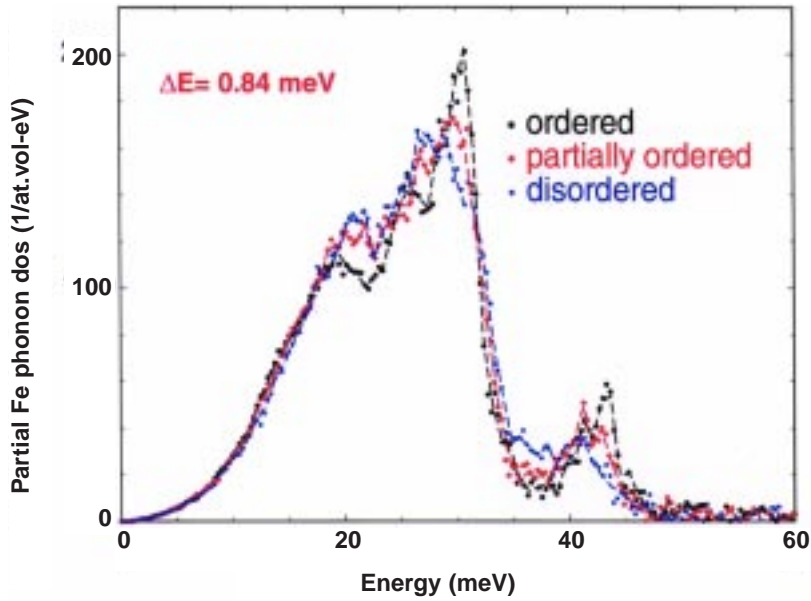


FIG. 6. Partial phonon density of states of Fe in Fe_3Al system as a function of order-disorder transformation. The systematic changes in the spectra indicate the effect of chemical short-range order on the vibrational dynamics of the alloy. The optical modes at 43 meV are due to Fe atoms with Al near neighbors. The sensitivity of phonon density of states to local ordering is somewhat of a surprise, given the general understanding that interatomic forces are of long range in metals. (Work done in collaboration with Prof. B. Fultz, California Institute of Technology.)

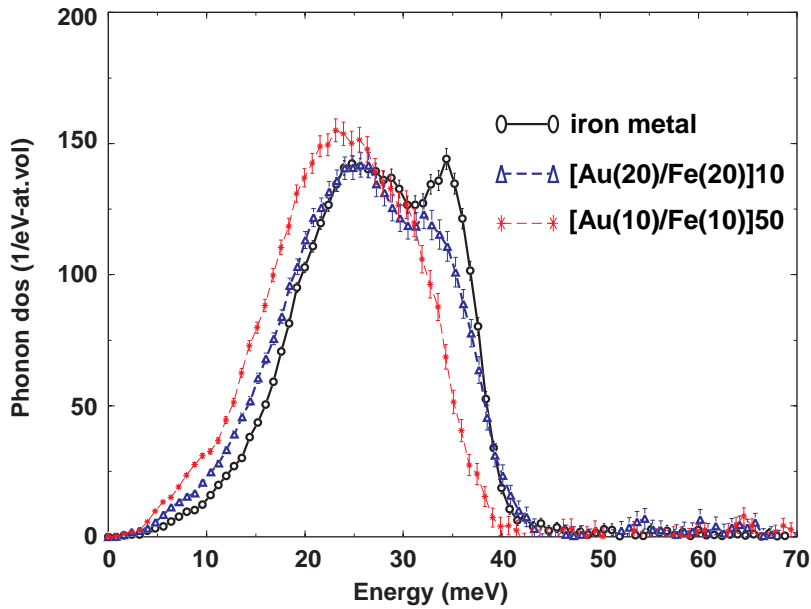


FIG. 7. Phonon density of states of Fe in an Fe/Au multilayer with varying thicknesses. As the layer thickness decreases, the softer modes below 25 meV appear to gain. Also note the disappearance of the longitudinal acoustic mode at 36 meV. Similar trends were observed with decreasing thickness in pure iron films. (Work in progress, in collaboration with S. Bader of Argonne National Laboratory.)

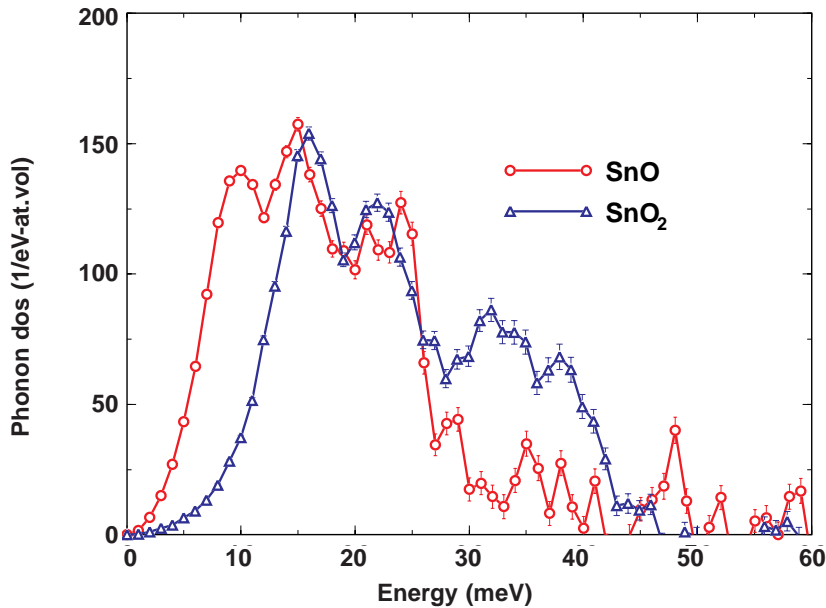


FIG. 8. Partial phonon density of states of Sn in two oxides, SnO and SnO_2 . The experiments allowed an accurate determination of Lamb-Mössbauer factors. For SnO the probability of recoil-free fraction of absorption and emission of 23.880 keV x-rays is 0.318 ± 0.041 , and for SnO_2 the same probability is 0.627 ± 0.09 .

cont'd from page 11

The inelastic scattering technique described above requires the use of single crystals. In order to study polycrystalline materials, powder samples, and, in particular, thin films, alternative methods must be developed. One such alternative is the use of nuclear resonance as an energy analysis technique. This approach was introduced in 1994,¹⁴⁻¹⁶ and it relies on tunable high-energy-resolution monochromators and the presence of suitable isotopes in the sample under analysis. This technique provides unequalled capability in terms of measuring partial phonon density of states in any medium, solid or liquid, crystalline or amorphous, bulk or thin films — even monolayers at an interface. It also allows extraction of phonon density of states directly from the data without the knowledge of crystal structure. New developments at the APS with respect to this technique are: (A) the resolution with which it can be carried out, (B) the media to which it can be applied, and (C) the isotopes for which optics have been produced.

(A) As shown in Table 1, we have developed the first sub-meV monochromator for lattice dynamic measurements. The dispersive, asymmetrically cut Si (975) crystals, shown in Fig. 4, yielded 0.66 meV ($\Delta E/E = 4.5 \times 10^{-8}$) resolution and 3×10^8 photons/sec at 14.4 keV. By using this monochro-

mator, phonon density of states of Fe metal has been measured and compared to theory derived from single-crystal neutron scattering measurements (Fig. 5).⁵ We have also made use of this monochromator to study the effect of order-disorder in an Fe₃Al system (Fig. 6).¹⁷

(B) We have demonstrated that this method can be utilized to study the effect of reduced dimensionality on vibrational modes. In this instance, we measured phonon density of states of nanocrystalline iron,¹⁸ and in thin films of Fe/Au multilayers, as shown in Fig. 7.

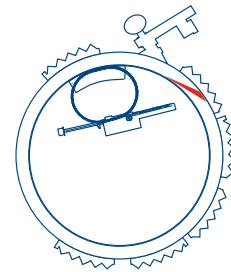
(C) It is our goal to widen the application of inelastic nuclear resonant scattering to other isotopes. Toward this end, we have built monochromators for ¹¹⁹Sn and ¹⁵¹Eu isotopes. The first results on Sn are shown in Fig. 8, in which the partial phonon density of states of SnO is compared to SnO₂. The ¹¹⁹Sn resonance was observed in September 1997. The resolution achieved was 3.4 meV at 23.878 keV ($\Delta E/E = 1.4 \times 10^{-7}$). The ¹⁵¹Eu resonance was observed in November 1997 with 1 meV resolution at 21.548 keV ($\Delta E/E = 4.6 \times 10^{-8}$).

The results presented here represent a small fraction of the work carried out at SRI-CAT. We encourage those with an interest in applying some of these methods to contact us directly. ○

REFERENCES

- 1 T. Toellner, Ph.D. Thesis, Northwestern University, 1996.
- 2 Program "DuMond" written by T. Mooney based on linearized Bragg equation as given by T. J. Davis, J. of X-Ray Science & Tech. **2**, 180 (1990).
- 3 Available from T. Toellner (APS), e-mail: toellner@aps.anl.gov.
- 4 N-beam program, written by R. Colella (Purdue University) available from J. Sutter (APS), e-mail: sutter@aps.anl.gov.
- 5 T. Toellner, M. Y. Hu, W. Sturhahn, K. Quast, and E. E. Alp, Appl. Phys. Lett **71**, 2112 (1997).
- 6 A. Chumakov, J. Metge, A. Q. R. Baron, H. Grunsteudel, H.F. Grunsteudel, R. Ruffer, and T. Ishikawa, et al, Nucl. Instr. Meth. A **383**, 642 (1996).
- 7 B. Dorner, E. Burkel, and J. Peisl, Nucl. Instr. Methods A **246**, 450 (1986).
- 8 E. Burkel et al, SPIE Conference Proceedings Vol. 1140, 426 (1989).
- 9 R. Verbeni, F. Sette, M. Krisch, U. Bergman, B. Gorges, C. Halcoussis, K. Martel, C. Masciovecchio, J. F. Ribois, G. Ruocco, and H. Sinn, J. Sync. Rad. **3**, 426 (1996).
- 10 M. Schwoerer-Böhning, P. Abbamonte, A. Macrander, and V. Kushnir, SPIE Conference Proceedings, vol 3151, 282 (1997).
- 11 T.M. Mooney, T. S. Toellner, W. Sturhahn, E. E. Alp, and S. D. Shastri, Nucl. Instr. Meth. A **347**, 348 (1994).
- 12 T. Ishikawa, Y. Yoda, K. Izumi, C. K. Suzuki, X. W. Zhang, M. Ando, and S. Kikuta, Rev. Sci. Instr. **63**, 1015(1992).
- 13 E. E. Alp, T. M. Mooney, and T. Toellner, U.S. Patent No. 5,524,040, issued on June 4, 1996.
- 14 M. Seto, Y. Yoda, S. Kikuta, X. W. Zhang, M. Ando, Phys. Rev. Lett. **74**, 3828 (1995).
- 15 W. Sturhahn, T. S. Toellner, E. E. Alp, X. W. Zhang, M. Ando, Y. Yoda, S. Kikuta, M. Seto, C. W. Kimball, and B. Dabrowski, Phys. Rev. Lett. **74**, 3832 (1995).
- 16 A. Chumakov, A.Q. R. Baron, R. Ruffer, H. Grunsteudel, H. F. Grunsteudel, and A. Meyer, Phys. Rev. Lett. **76**, 4258(1996).
- 17 B. Fultz, T. A. Stephens, W. Sturhahn, T. S. Toellner, and E. E. Alp, (Submitted for publication in Phys. Rev. Lett.).
- 18 B. Fultz, C. C. Ahn, E. E. Alp, W. Sturhahn, T. Toellner, Phys. Rev. Lett **79**, 937 (1997).

X-RAY IMAGING & MICROSPECTROSCOPY OF THE MYCORRHIZAL FUNGUS-PLANT SYMBIOSIS



ZHONGHOU CAI^{*}, WENBING YUN^{*}, STEPHEN T. PRATT,[†] RAYMOND M. MILLER[†],
EFIM GLUSKIN^{*}, DOUGLAS B. HUNTER[‡], AMIEL G. JARSTFER[§], KENNETH M. KEMNER[†],
BARRY LAI^{*}, HEUNG-RAE LEE^{*}, DANIEL G. LEGNINI^{*}, WILLIAM RODRIGUES^{*},
& CHRISTOPHER I. SMITH[†]

^{*}Experimental Facilities Division, Argonne National Laboratory • [†]Environmental Research Division, Argonne National Laboratory • [‡]Savannah River Ecology Laboratory, The University of Georgia • [§]LeTourneau University



The scanning microprobe (right) at beamline 2-ID-D joins the high brilliance of an Advanced Photon Source undulator source to the high performance of a phase zone plate as a microfocusing device. The microprobe is demonstrating unprecedented submicron spatial resolving power that can be used in a wide range of x-ray applications. A focal spot of less than $0.25 \mu\text{m}$ (FWHM) has been demonstrated, and a photon flux density exceeding $5 \times 10^{10}/\text{sec}/\mu\text{m}^2/0.01\% \text{BW}$ has been obtained. The microprobe can simultaneously perform x-ray diffraction microscopy, fluorescence microscopy, spectromicroscopy, and 3D tomography with submicron spatial resolution. It has been used for a broad range of applications since commissioning in December of 1996, including the study of plant roots and fungi (described in this article), platinum-based anti-cancer agents, integrated laser/modulator microdevices, electromigration in Al wires in semiconductor devices, submicron spatial resolution and three-dimensional tomography of a single mammalian cell.

X-ray fluorescence microscopy (XFM) and microspectroscopy with unprecedented capabilities at micron spatial resolution have been developed on the 2-ID-D/E hard x-ray beamline at the Advanced Photon Source (APS) and applied to the study of the symbiotic relationship between mycorrhizal fungi and plants. These new capabilities for the study of biological and environmental samples couple high-brilliance synchrotron radiation and high-performance x-ray microfocusing optics to the intrinsic advantages of x-rays for element mapping and chemical-state imaging.

Approximately 90% of the world's vascular plants, including the majority of all economic crops, belong to families that commonly have symbiotic associations with mycorrhizal fungi.^{1,2} While such associations are known to increase plant viability under low nutrient conditions, in some instances mycorrhizal fungi can also moderate toxicity effects in plants growing in soils containing elevated concentrations of heavy metals.^{3,4} Thus, an improved understanding of the plant-fungus relationship, particularly with respect to the uptake mechanisms

for metals, is expected to have significant implications in both agriculture and the remediation and restoration of contaminated environments.

X-ray fluorescence microscopy and microspectroscopy can provide information on the spatial distribution, oxidation state, chemical environment, and chemical transformations of trace elements.⁵⁻¹⁰ In comparison with electron and proton microprobes,¹⁰ the cross sections of x-ray fluorescence excited by x-rays are typically 10 to 10^3 times higher than those excited by charged particles, and the

fluorescence signal-to-background ratios are 10 to 10^5 times better for excitation by x-rays. Although the spatial resolution of electron and proton microprobes can approach molecular dimensions and is better than that achievable with x-rays, the elemental sensitivity is limited to approximately 100 ppm for electron-induced x-ray microanalysis and 10 ppm for proton-induced x-ray microanalysis, considerably worse than with x-rays.¹¹ In addition, the energy deposition for x-rays is 10^3 to 10^5 times smaller for a given elemental detectability,¹⁰ resulting in substantially less radiation damage to the sample. Moreover, sample preparations for x-ray microprobes are far simpler than those for charged-particle microprobes, making it possible to study samples in their natural hydration states, which is not possible using charged-particle microprobes. With charged-particle microprobes, the samples must be stained and thinned to improve both contrast and signal-to-noise ratio, coated with a thin conducting layer to reduce charging effects and improve spatial resolution, and be in vacuum to maintain the charged-particle beams. Finally, information on the chemical state of the detected elements is difficult to obtain using techniques based on charged particles.

In recent years, soft x-ray (<1 keV) microscopy and spectromicroscopy have been successfully used for the study of biological samples.⁵ However, higher energy x-rays are required to access the K edge of the third-row and heavier elements in the periodic table, many of which are either important nutrients, micronutrients, or contaminants with potentially toxic effects. The fluorescence yield for high-energy x-rays is also significantly greater than that for soft x-rays (it can be much less than 1%), and hard x-rays suffer considerably less attenuation along the optical path to and from the sample. The improvement in hard x-ray imaging and microspectroscopy techniques is expected to have important implications for the study of biological and environmental systems.

The high brilliance of third-generation synchrotron sources and developments in microfabrication technologies for high-resolution and high-efficiency hard x-ray zone plates¹² have resulted in substantial advances in the state of the art in x-ray spectromicroscopy, fluorescence microscopy, and phase contrast imaging. In this article, we report recent experimental results, obtained at the 2-ID-D/E beamline of the APS,¹³ illustrating these capabilities by hard x-ray phase contrast imaging, XRF imaging, and microspectroscopy of mycorrhizal plant roots and fungi in their natural hydrated states. The XRF microprobe is demonstrated by the simultaneous mapping of the elemental distributions of P, S, K, Ca, Mn, Fe, Ni, Cu, and Zn with a spatial resolution of approximately $1 \times 3 \mu\text{m}$ and

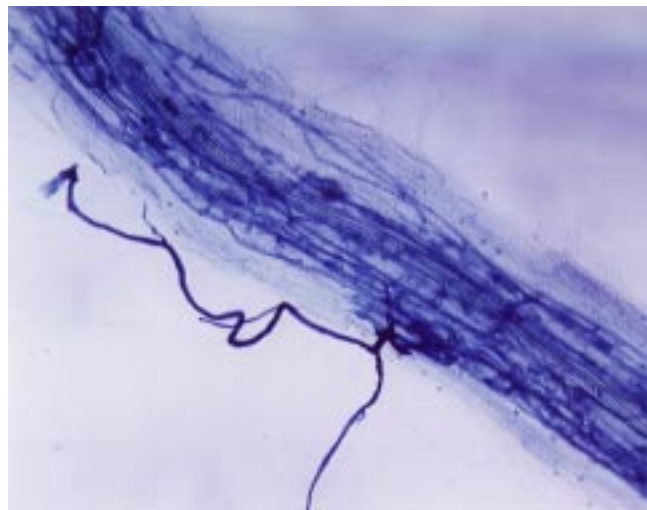


FIG 1(a). An optical micrograph of a clarified and stained *P. lanceolata* root infected by the mycorrhizal fungus *Glomus mosseae*.

with an elemental sensitivity of approximately 10 ppb. Microspectroscopy with the same spatial resolution is demonstrated by recording near-edge x-ray absorption (XANES) spectra of Mn at a concentration of approximately 3 ppm. These results specifically address the uptake mechanisms of metals by mycorrhizal plants and fungi.

An optical micrograph of a *Plantago lanceolata* L. root that has been infected by the arbuscular mycorrhizal fungus *Glomus mosseae* is shown in Fig. 1(a). X-ray phase contrast imaging provides a particularly effective method for imaging the sample and locating suitable regions of interest for fluorescence mapping and micro-XANES measurements. Phase contrast images were recorded by using a combination of scintillation crystal and charge-coupled-device detector system. Because the absorption contrast of the root-fungus sample at the x-ray energy (11.9 keV) used in the experiments is essentially invisible, the phase change when the x-rays pass through the sample provides the main contrast for the image. Figure 1(b) shows a phase contrast image of a hydrated plant root infected with the mycorrhizal fungus. The dark structure through the center of the root is a well-formed stele, which is indicative of the hydrated state of the root. A phase contrast image of an air-dried root (not shown) shows a shriveled and collapsed stele. The threadlike features coming off approximately perpendicular to the root are fungal hyphae. The hyphae can be distinguished from root hairs because they branch and enter the root at multiple points.

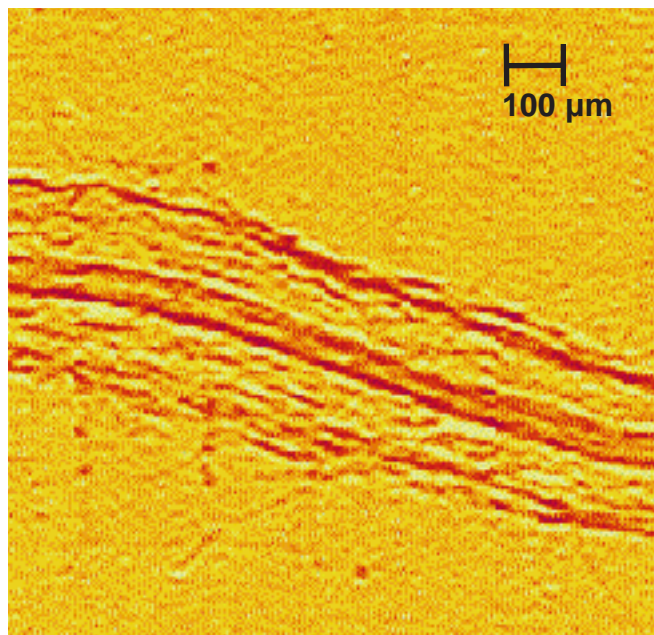


FIG. 1(b). A hard x-ray phase contrast image of an unclarified, unstained, wet *P. lanceolata* root infected by the mycorrhizal fungus *Glomus mosseae*.

The spatial resolution of the images in Fig. 1(a) and 1(b) is comparable; as a point of reference, an average root cell is approximately 80 μm in length and 30 μm in diameter. Similar features are observed in the optical and phase contrast images. It must be stressed, however, that the optical image of Fig. 1(a) required substantial sample preparation, while the phase contrast image of Fig. 1(b) required essentially none and could even be applied to living plants. Thus, the phase contrast image shows structures that could be lost or altered in the preparation of the sample for optical imaging. Nevertheless, a more detailed comparison of optical images and hard x-ray phase contrast images is expected to be informative, especially when the phase contrast images are recorded near the K edges of selected elements of interest, which will provide some elemental selectivity. The simplicity and short exposure times of the phase contrast method make it an extremely useful tool for positioning the sample for XRF imaging and microspectroscopy.

The XRF-imaging and microspectroscopy experiments were performed using a focused x-ray beam of 11.9 keV, with a zone plate of $1\ \mu\text{m} \times 3\ \mu\text{m}$ cross section and 3×10^{10} photons/s/0.01% BW. A schematic of the beamline apparatus is shown in Fig 2. Samples for the XRF images were mounted at 45° to the incident beam, and the $3\text{-}\mu\text{m}$ -wide horizontal beam projected on the sample $4.2\ \mu\text{m}$ approximately while the $1\ \mu\text{m}$ vertical dimension of the beam was preserved. In order to take advantage of the polarization of the synchrotron radiation and to

reduce the background, x-ray fluorescence from the sample was monitored at 90° to the incident beam horizontally by using an energy-dispersive detector. The integrated intensities of the $K\alpha$ fluorescence corresponding to individual elements were measured as functions of the sample's vertical and horizontal positions with $5\ \mu\text{m}$ steps and collection time of 3 seconds for each point. Although this means that the image was somewhat under sampled in the vertical dimension, this step size was necessary to image the desired regions of the sample with reasonable data-acquisition times. The total data-collection time for a 61×61 pixel array ($300 \times 300\ \mu\text{m}^2$) was approximately 4 h.

Figure 3 shows a series of images of a wet fungus sample analyzed for the micronutrients Mn, Fe, Cu, and Zn. Similar images have been recorded for the nutrients P, K, S, Ca, and Ni. The absolute element concentrations were determined by calibrating the detector with standard films. The nutritional requirements for elements can be divided into two concentration classes: macronutrients, required at about 10^{-3} M, and micronutrients, required at 10^{-6} M or less.² The macronutrients measured in this study were P, K, S, and Ca; the micronutrients were Fe, Mn, Cu, Zn. We also measured Ni, a metal normally considered toxic at high concentrations.

The distributions of the four micronutrients in Fig. 3 show different behavior. Interestingly, there is little evidence for Mn in the fungal hyphae, which may be related to the observation that mycorrhizal plants typically have much lower Mn concentrations than non-mycorrhizal plants.² The Fe tends to be most concentrated at the edge of the root, perhaps reflecting the precipitation of Fe in this location. Both Cu and Zn show up most strongly in the fungal hyphae and in the center of the root, most likely in the inner cortex where the proliferation of the fungus is greatest (see Fig. 1[a]). This suggests the use of Cu and Zn as surrogate measures of mycorrhizal fungi in roots.

With only a few exceptions, images of even completely dried roots show features similar to those in the hydrated root of Fig. 3. One striking contrast between the dry and wet samples is the significantly smaller amount of K in the fungal hyphae of the dried sample. Although the present results do not indicate whether the K moves into the root or to the outside of the hyphae, the mobilization of K upon drying of the sample could have important implications in the development of remediation technologies. More specifically, fungi are particularly effective in taking up Cs from soils, and their use in the sequestration and removal of radioactive Cs from contaminated sites has been discussed.¹⁴ If Cs, like K, is mobilized upon drying, the effectiveness of the remediation strategy could be compromised. Efforts to characterize Cs uptake and mobility are

currently under way. The observations for K also illustrate the potential of the x-ray imaging techniques described here for the study of dynamical and transport processes in biological systems.

Although the XRF images of Fig. 3 provide detailed information on the spatial distributions of selected elements, they provide no information on the chemical states or local environments of the elements. To further demonstrate the capabilities of the x-ray microprobe, we recorded micro-x-ray absorption near-edge structure (XANES) spectra at the Mn K edge with a $1 \times 3 \mu\text{m}$ spot size at a selected area within the sample shown in Figs. 1(b) and 2. Mn is an essential micronutrient in both plants and fungi, and in natural systems it usually exists in the +2 or +4 oxidation state (the +3 oxidation state is also possible but generally unstable). The +2 oxidation state is soluble and is the form that is most useful to plants and fungi.² The +4 oxidation state is insoluble and has less biological importance. The small beam size used in these experiments ensured that a single fungal hypha can be studied if desired.

The XANES spectra were obtained by positioning an interesting feature of the sample in the focused x-ray beam and scanning the x-ray energy through the absorption edge while monitoring the Mn $K\alpha$ fluorescence. Figure 4 shows a Mn micro-XANES spectrum with the beam aligned to the stele in the center of the root. Each point in the spectrum was averaged for 10 s of detector live time, and the full spectrum was recorded in approximately 45 min. The spectrum has been normalized by the intensity of the transmitted light. XANES spectra were recorded in a variety of locations across the sample, including the root cortex and the extramatrical fungal hyphae. In this sample, the Mn XANES spectrum was found to be independent of position, and all of the spectra were essentially indistinguish-

able from the one in Fig. 4. (Spectra on the fungal hyphae were somewhat noisier as a result of the small amount of hyphal material.) Comparison of our results with detailed XANES studies of a wide variety of samples and standards^{15,16} indicated that at least 90% of the Mn sampled by the x-ray beam at each of the locations is Mn^{+2} . This is clear from the sharp rise at threshold and the relatively intense white line, as opposed to the gradual onset and weak white line observed in Mn^{+4} . Although the observation of Mn^{+2} in the present sample is not surprising, the results demonstrate the ability to record high-quality XANES spectra with $1 \times 3 \mu\text{m}$ spatial resolution. In principle, similar measurements for other third-row and heavier elements should be straightforward.

The combination of high-brilliance synchrotron radiation from the APS and high-performance zone plates provides substantial improvements in the state of the art of hard x-ray phase contrast imaging, XRF imaging, and micro-XANES spectroscopy of biological and environmental samples. Hard x-ray phase contrast imaging was shown here to provide a straightforward, sensitive, high-resolution method for imaging biological samples with minimal radiation damage. XRF imaging at the APS can now be performed with monochromatic radiation, resulting in a substantial reduction in background due to scattered radiation. New zone plates should soon allow element-specific, hard x-ray XRF imaging with submicron spatial resolution. Although the benefits to phase contrast imaging and XRF imaging are substantial, perhaps the most striking advance is the decrease by a factor of approximately 100 in the beam size. This makes microspectroscopy techniques useful for gathering information on the chemical states and local environments of elements on a scale compatible with a

cont'd on page 20

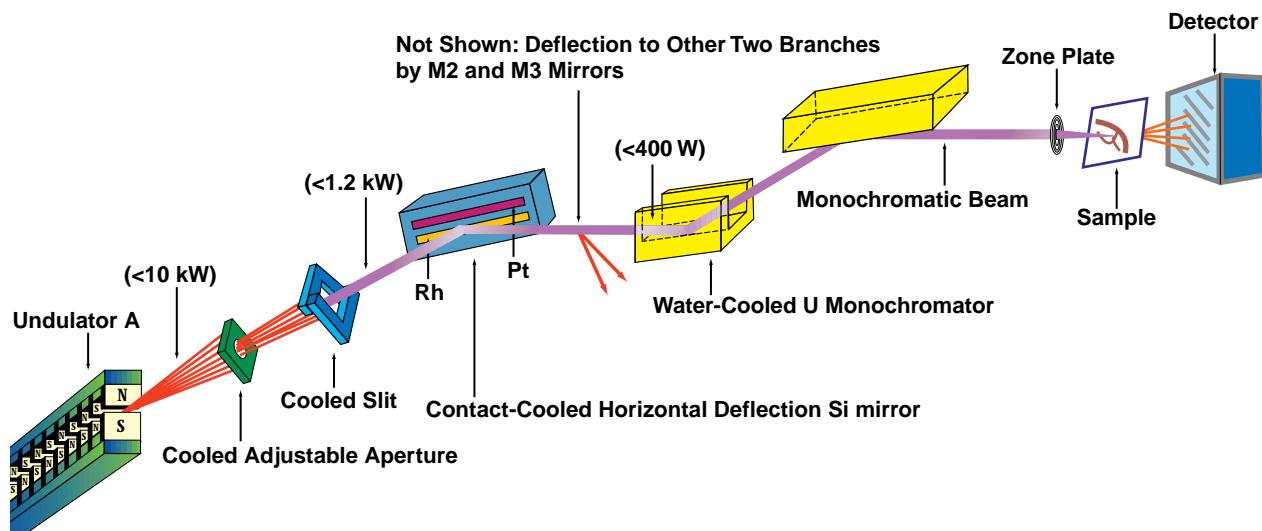
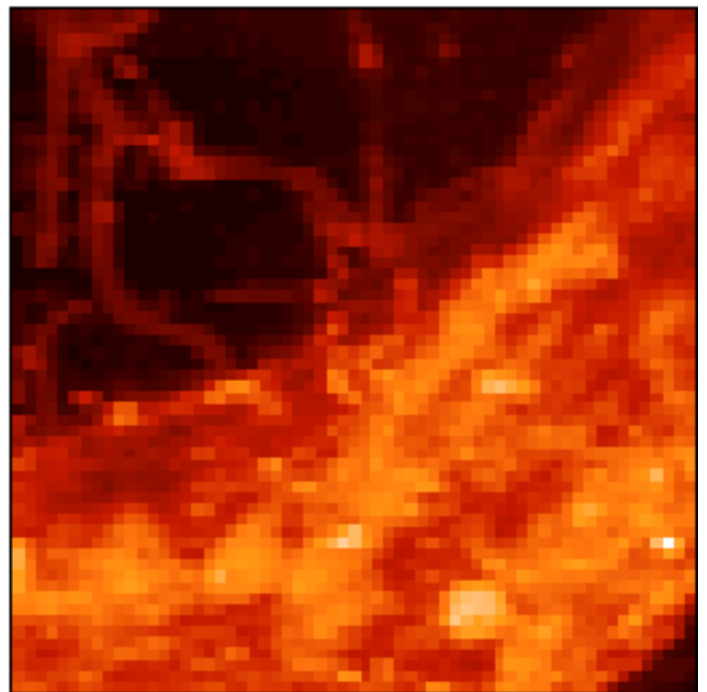
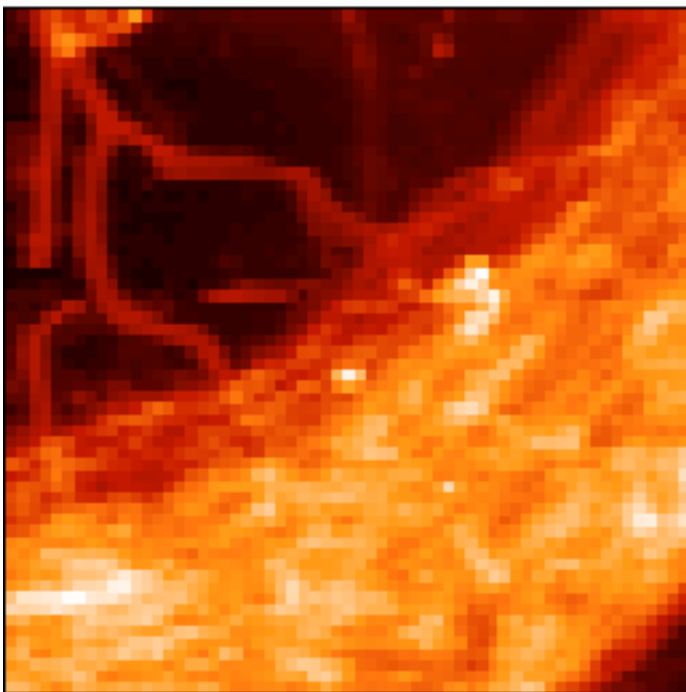
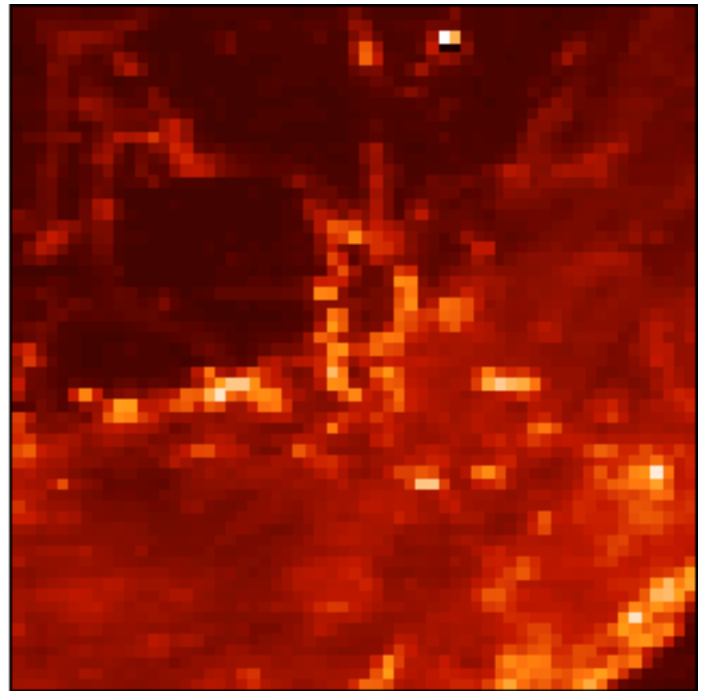
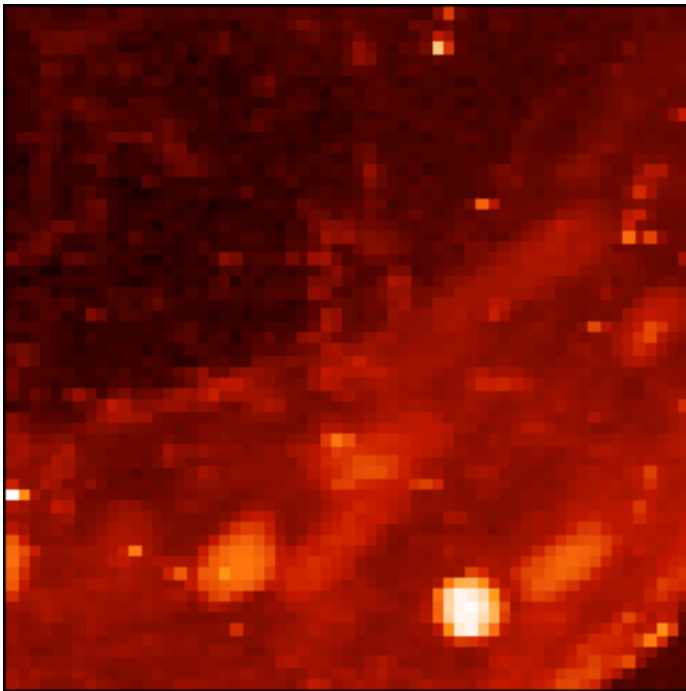


FIG. 2. One of three branches on the 2-ID D/E - Sector 2, insertion device branch line.

Mn: 0.03 to 0.87 $\mu\text{g}/\text{cm}^2$

Fe: 0.11 to 27.9 $\mu\text{g}/\text{cm}^2$



Cu: 0.03 to 1.55 $\mu\text{g}/\text{cm}^2$

Zn: 0.04 to 4.98 $\mu\text{g}/\text{cm}^2$

300x300 μm area
5x5 μm pixels

Min.



Max.

FIG. 3. Selected element-specific XRF images of a hydrated *P. lanceolata* root infected by the mycorrhizal fungus *G. mosseae*. This is a portion of the root shown in the phase contrast image in Fig. 1(b).

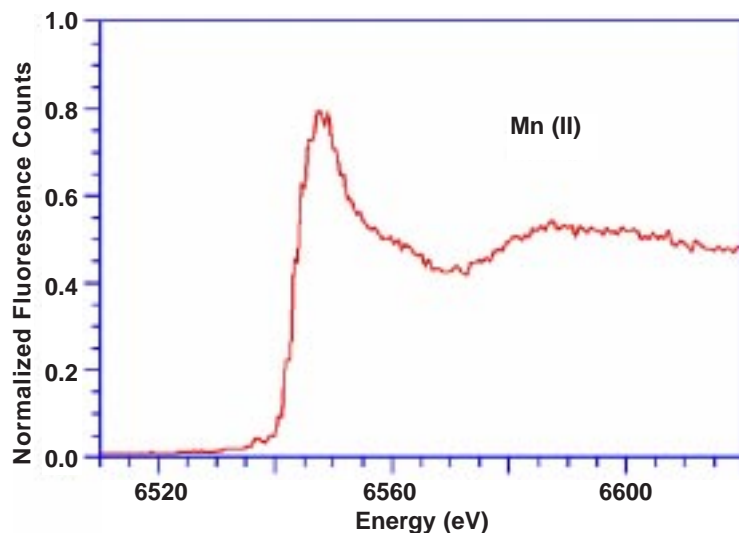


FIG. 4. The micro-XANES spectrum at the Mn K edge obtained with a $1\ \mu\text{m} \times 3\ \mu\text{m}$ focal spot aligned to the stele in the central portion of the root shown in Fig. 1(b). Comparison of the spectrum with known standards indicates that at least 90% of the Mn is in the +2 oxidation state.

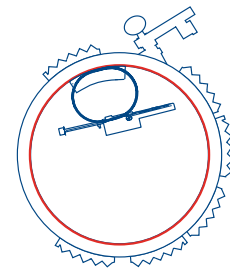
cont'd from page 18

variety of important biological and cellular structures. The commissioning of new imaging beamlines at the APS and other third-generation synchrotron sources is expected to result in a rapid development of capabilities to address issues in the biological and environmental sciences. ○

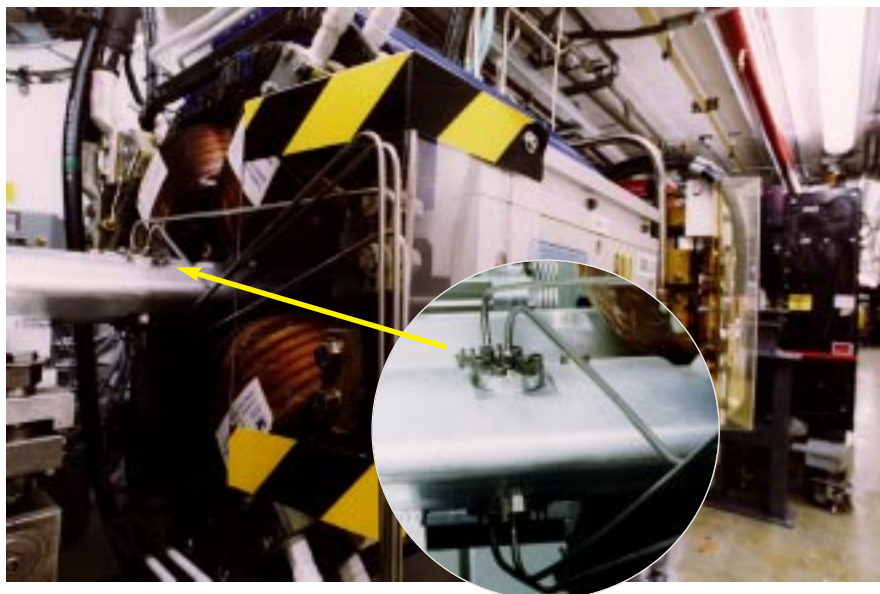
REFERENCES

- ¹ M. F. Allen, *The Ecology of Mycorrhizae* (Cambridge University Press, New York, 1991).
- ² H. Marschner, *Mineral Nutrition of Higher Plants*, Second Edition (Academic Press, New York, 1995).
- ³ R. Bradley, A. J. Burt, and D. J. Read, *Nature* **292**, 335 (1981); R. Bradley, A. J. Burt, and D. J. Read, *New Phytol.* **91**, 197 (1982).
- ⁴ U. Galli, H. Schüepp, and C. Brunold, *Physiol. Plantarum* **92**, 364 (1994).
- ⁵ J. Kirz, C. Jacobsen, and M. Howells, *Quart. Rev. Biophys.* **28**, 33 (1995).
- ⁶ S. V. Mattigod, M. L. Rivers, and S. R. Sutton, in *Synchrotron X-Ray Sources and New Opportunities in the Soil and Environmental Sciences: Workshop Report*, edited by D. G. Schulze and J. V. Smith, Argonne National Laboratory Report ANL/APS/TM-7, 101 (July 1990).
- ⁷ D. G. Schulze and P. M. Bertsch, *Adv. Agron.* **55**, 1 (1995).
- ⁸ P. M. Bertsch, D. B. Hunter, S. R. Sutton, S. Bajt, and M. L. Rivers, *Environ. Sci. Technol.* **28**, 980 (1994).
- ⁹ See, for example, D. C. Koningsberger and R. Prins, *X-Ray Absorption: Principles, Applications, Techniques of EXAFS, SEXAFS, and XANES* (Wiley, New York, 1988).
- ¹⁰ C. J. Sparks, Jr., in *Synchrotron Radiation Research*, edited by H. Winick and S. Doniach (Plenum Press, New York, 1980) p. 459.
- ¹¹ B. Forslind, K. G. Malmquist, and J. Pallon, *Scanning Microscopy* **5**, 877 (1991).
- ¹² B. Lai, W. Yun, D. Legnini, Y. Xiao, J. Chrzas, P.J. Viccaro, V. White, S. Bajikar, D. Denton, and F. Cerrina, *App. Phys. Lett.* **61**, 1877 (1992).
- ¹³ W. Yun, B. Lai, D. Shu, A. Khounsary, Z. Cai, J. Barraza, and D. Legnini, *Rev. Sci. Instrum.* **67**, (9) CD-ROM.
- ¹⁴ K. Haselwandter, M. Berreck, and P. Brunner, *Trans. Br. Mycol. Soc.* **90**, 171 (1988); G. M. Clint, J. Dighton, and S. Rees, *Mycol. Res.* **95**, 1047 (1991); J. Dighton, G. M. Clint, and J. Poskitt, *Mycol. Res.* **95**, 1052 (1991).
- ¹⁵ D. G. Schulze, T. McCay-Buis, S. R. Sutton, and D. M. Huber, *Phytopathol.* **85**, 990 (1995); D. G. Schulze, S. R. Sutton, and S. Bajt, *Soil Sci. Soc. Am. J.* **59**, 1540 (1995).
- ¹⁶ A. Manceau, A. I. Gorshkov, and V. A. Drits, *Am. Mineralogist* **77**, 1133 (1992); A. Manceau, A. I. Gorshkov, and V. A. Drits, *Am. Mineralogist* **77**, 1144 (1992).

MEASUREMENT & CONTROL OF PARTICLE-BEAM TRAJECTORIES IN THE ADVANCED PHOTON SOURCE STORAGE RING



Glenn Decker *Accelerator Systems Division, Argonne National Laboratory*



In order to provide Advanced Photon Source (APS) users with stable x-ray beams, it is necessary that undesirable beam motions be eliminated at the source, i.e., from the positron beam in the storage ring. This article is a review of the stability objectives, position measurement techniques and capabilities, and AC and DC orbit servo techniques used at the APS. A summary of performance to date is given, along with a brief discussion of the performance limitations of the present system and upgrade plans for improving upon these limits.

STABILITY SPECIFICATIONS

The orbit stability requirements for the APS storage ring were specified during the accelerator-design phase. In order to provide stable x-ray beams, the rms beam motion must be less than 5% of the particle-beam dimensions at the source point. For insertion device sources, given the design values for ring emittance and coupling, this requirement is summarized as:

$$\Delta x < 17.3 \text{ mm rms}, \Delta x' < 1.22 \text{ } \mu\text{rad rms}$$

$$\Delta y < 4.5 \text{ mm rms}, \Delta y' < 0.45 \text{ } \mu\text{rad rms}$$

where Δx and $\Delta x'$ are the tolerances for horizontal displacement and angular motion, respectively, and Δy and $\Delta y'$ are the corresponding vertical tolerances. Keep in mind that the thickness of a human hair is typically about $50 \text{ } \mu\text{m}$. Note also that the position and angle tolerances in general are not independent quantities; a relation can be derived from the magnetic lattice to show that the ratio of the rms position and angle motion is fixed for noise sources occurring randomly around the ring.

ORBIT MEASUREMENT¹

The primary diagnostic used for control of the orbit in the APS storage ring (large photo above) are the radio frequency (rf) beam position monitors (Fig. 1 next page), commonly referred to as rf BPMs. Capacitive button pickup electrodes mounted on the

vacuum chamber (circular photo above) provide signals to in-tunnel differencing/filtering electronics. These "filter-comparator" units transmit rf frequency difference and sum signals derived from the four buttons at each of 360 rf BPM stations to rf monopulse receivers ("amplitude to phase," or AM-PM converters) placed on top of the storage ring tunnel enclosure and connected using low-loss coaxial cables (Andrews FSJ1-50 heliax). The monopulse receivers effectively normalize these signals (difference/sum), supplying video bandwidth ($\sim 10 \text{ MHz}$) signals to the digitizer, which are proportional to transverse beam position. Beam position information is digitized once per turn with 12 bits of resolution.

Following digitization, the data are averaged both with hardware circuitry and special software that runs in a nearby Experimental Physics and Industrial Control System (EPICS) input/output controller (IOC). The result is a measure of beam position with submicron resolution, albeit with very limited bandwidth. Typically, the computer-driven orbit control algorithms will eliminate orbit "drift" with variations slower than some tens of seconds. Beam jitter is removed using the real-time orbit feedback system, described below. The real-time system makes use of the same position information, but without any EPICS software averaging, instead having its own hardware averager.

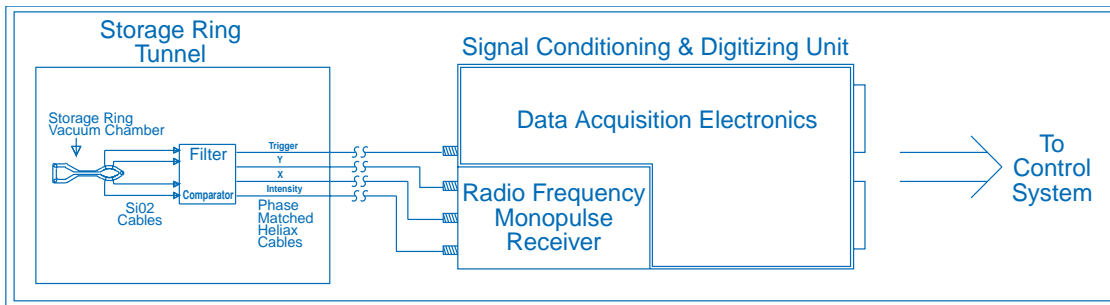


FIG. 1. Block diagram of the APS storage ring beam position monitor system.

DC ORBIT CONTROL²

Once the 720 pieces of beam position information (360 in each plane) are available to EPICS, a sophisticated software algorithm uses them to compute corrections to apply to the control setpoints of a subset of the 317 available combined function horizontal/vertical corrector magnets. Essentially, the change in position Δx at each of the 360 BPM stations is related to the change in the vector of 317 corrector settings ΔC_x via a rather large, unsymmetrical response matrix \mathbf{R} as follows:

$$\mathbf{R} \Delta C_x = \Delta x,$$

and similarly for the vertical plane. In principle, one can simply invert the matrix, which is straightforward given available algorithms like singular value decomposition, and send a resultant vector of corrector setpoints in such a way as to minimize the rms of the readbacks from the 360 BPMs.

Practically speaking, it is most difficult to perform useful correction of slow orbit drift, primarily as a result of very small but significant systematic errors. The systematic errors faced by the APS orbit control system are typically on the scale of tens of microns, derived both from mechanical sources, such as the response of the vacuum chamber to temperature changes, and from variations in the properties of the processing electronics resulting from changes in beam intensity, temperature, etc.

To compensate for these systematic errors, several things are done inside the DC orbit-correction algorithm. Only a small number of correctors are chosen, typically about 60 out of the 317 possible, while as many BPM readbacks as possible are used for global correction. The remainder of the correctors that are not used for DC orbit correction are generally used for local beamline steering, which is done infrequently. Overdetermining the orbit correction in this manner has the result of correcting very efficiently long spatial wavelength (i.e., physical) beam motions while tending to ignore the unit-to-unit variations typically associated with systematic effects. Shown in Fig. 2 is a typical display containing horizontal and vertical beam position data, actually a difference measured relative to a reference data set. Note that the beam motion generally has a

strong 35th harmonic in the horizontal plane and a longer wavelength 14th harmonic in the vertical, corresponding to the machine tunes of 35.2 and 14.3, respectively. Note also the presence of a small number of data points that do not fit the curve. These represent the types of systematic errors with which the orbit correction must deal. The benefit of taking advantage of statistics by using large numbers of BPMs cannot be overstated. Small systematic errors are reduced significantly in terms of their effect on real beam motion.

A “de-spiking” algorithm is used to eliminate suddenly misbehaving BPMs, or those which drift excessively, as demonstrated by Fig. 2. The erroneous readback is replaced by the average of neighboring units, which is made possible by the high density of BPMs around the ring. This avoids the necessity of recomputing the inverse response matrix, which, while formally more correct, requires interrupting the correction process so that new parameters may be calculated. Typically, any BPM whose “error” readback varies by more than 20 microns from neighboring units gets de-spiked. (A BPM error in this context has the connotation of being the deviation of a readback from its setpoint.)

Recall that the BPM electronics are self-normalizing, i.e., their readback is designed to be independent of the amount of beam stored. While this normalization is done with good accuracy, it is still

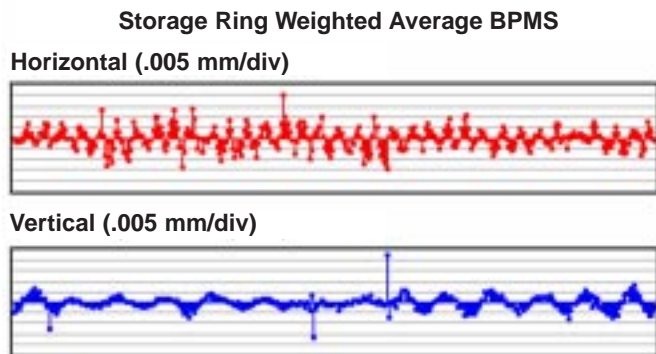


FIG. 2. Difference orbit showing typical global beam motion and systematic error effects. The vertical scale is $5 \mu\text{m}/\text{division}$.

not quite good enough. In fact, variations in position readback are seen at the tens of microns level in the absence of any true beam motion. This is characteristic of most rf BPM systems—systematic intensity compensation is routinely performed at the European Synchrotron Radiation Facility (ESRF), for example, to correct errors of magnitude similar to what is experienced at the APS.³ The variation in position with beam intensity is eliminated by a separate computer program that subtracts previously measured offset vs. intensity data from the position readbacks to provide a true, or adjusted, readback that is then fed into the orbit-correction algorithm.

A separate type of correction is now performed routinely that does not involve the steering corrector magnets at all. Twice a day, as the moon passes overhead (or underfoot), the circumference of the storage ring changes by about thirty microns due to Earth tides. In order to compensate for this, the frequency of the rf system is adjusted to regulate the orbit circumference. If left uncorrected, this effect would impact horizontal beam position in bending magnet beamlines.

AC ORBIT CONTROL⁴

An elaborate real-time feedback system has been implemented at the APS to handle AC orbit correction (Fig. 3). The system is all digital and relies on a distributed array of digital signal processors (DSPs) to perform corrections to the orbit at a 1-kHz rate. Digital data are sent directly from the BPM electronics to a crate of processing electronics. These data are then distributed to 20 other crates around the ring in real time by a dedicated fiber-optic network using a piece of hardware called a “reflective memory.” All local feedback crates thus have access to global data. The correction proceeds in much the same way as for the DC correction, but at a much faster data rate. Digital signal processors multiply columns of an inverse response matrix by the real-time position data to arrive at steering corrector setpoints. These setpoints are then digitally filtered to avoid overlapping the correction bandwidth of the DC correction and to optimize performance up to 30 Hz. The strategy used by the AC feedback is similar to the one used for DC correction in that a large number of BPMs (160) and a relatively small number of correctors (38 in each plane) are employed. Here the limitation on the number of BPMs is a matter of DSP processing speed.

One advantage that the real-time system has over the DC orbit correction is that the systematic errors are much less severe since the real-time system in its present implementation explicitly does not perform DC corrections. Thus, long-term drift effects are of much less importance. Strategies for dealing with systematic errors and malfunctioning BPMs are still under development. These are pri-

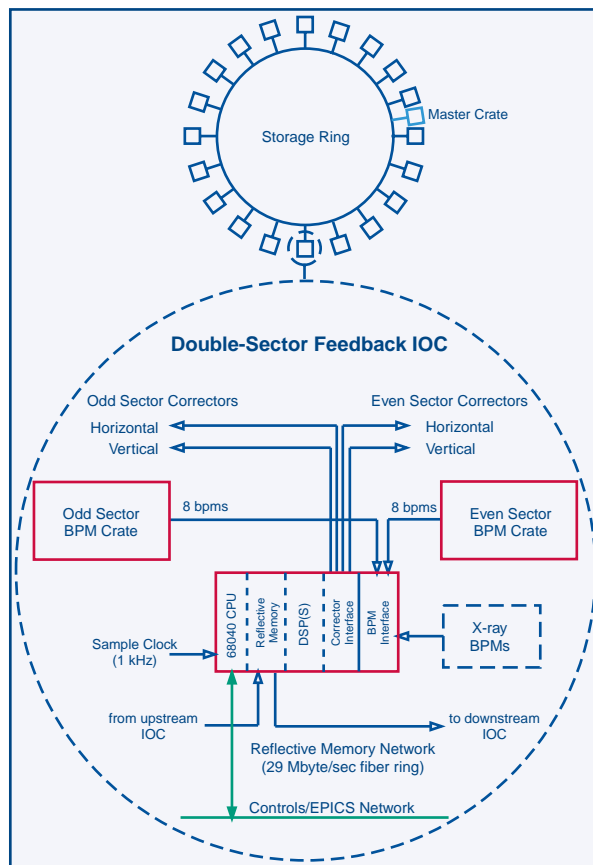


FIG. 3. Block diagram of the APS real-time closed-orbit feedback system.

marily a reliability issue for the system in terms of degraded beam parameters when the system must be turned off for reconfiguration to remove any malfunctioning BPMs from the algorithm.

In addition to reducing beam jitter, the real-time feedback has proven to be an extremely powerful tool in the effort to localize and eliminate noise sources. This is now beyond proof of principle—studies shifts have been routinely scheduled with the express purpose of tracking down, for example, noisy power supplies, which are then repaired. Transient noise sources, which are notoriously difficult to identify let alone eliminate, can be routinely monitored with the feedback system. The evidence is very promising that this technique will ultimately provide the lowest possible ambient noise level in the beam.

SYSTEM PERFORMANCE⁵

The result of orbit correction efforts to date are summarized in Figs. 4, 5, and 6. Figures 4 and 5 show power spectral densities for horizontal and vertical beam motion, respectively. Each spectrum is the average of data from 40 beam position monitors located near insertion device source points. The dimensions (mm^2/Hz) may be unfamiliar to some; however, the interpretation can be understood by recognizing that the area under the curve (on a lin-

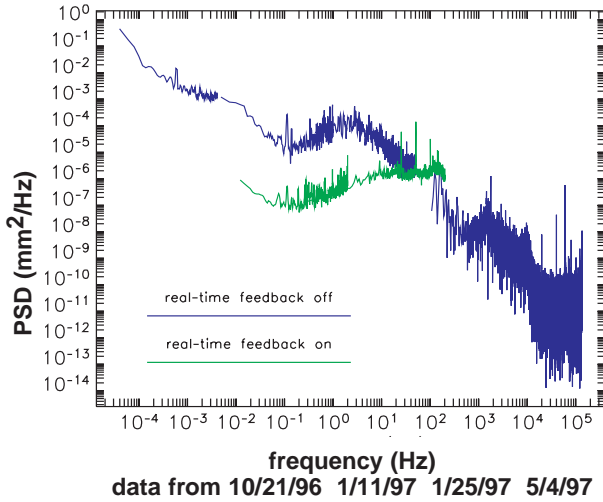


Fig. 4: APS horizontal beam-motion power spectral density at insertion device source points.

ear scale) yields the mean square beam motion. Notice that nearly ten decades of frequency are encompassed in the plots, ranging from data acquired over a 14-hour fill (2×10^{-5} Hz) all the way up to 135 kHz, which is the Nyquist frequency for data sampled once per revolution. The spectral peak at 0.0005 Hz corresponds to a 30-minute water temperature cycle. Between 0.1 and 0.2 Hz are two lines: one is the DC orbit correction sending corrections to the power supplies every ten seconds or so, and the other is the intensity dependence correction software. The narrow lines at 25, 50, and 75 Hz were traced to an unstable quadrupole magnet power supply, which has since been repaired. At 1.7 kHz, one can see the synchrotron tune — evidence of frequency modulation, i.e., variations in the beam’s revolution period. Finally, the lines at 20, 40, and 60 kHz correspond to the ubiquitous power supply “chopper noise” resulting from the pulse-width modulation regulators used for nearly all storage ring magnets.

The effects of the real-time feedback are clearly shown. It has the largest effect in the band ranging from a fraction of a Hz up to about 30 Hz, where a majority of the orbit motion occurs. Note that the very-low-frequency components, in addition to being the largest (in density), are also the most difficult to measure (it takes hours or even days) and are similarly very difficult to correct. Having said that, the progress in fill-to-fill and day-to-day orbit reproducibility has been very good, typically better than 10 microns rms vertically and similarly in the horizontal plane.

Shown in Fig. 6 is a more pedestrian view of the rate of improvement of orbit stability in the APS storage ring. Here the vertical axis corresponds to the rms beam motion in the band from 0.01 Hz up to 30 Hz, as a function of time measured by opera-

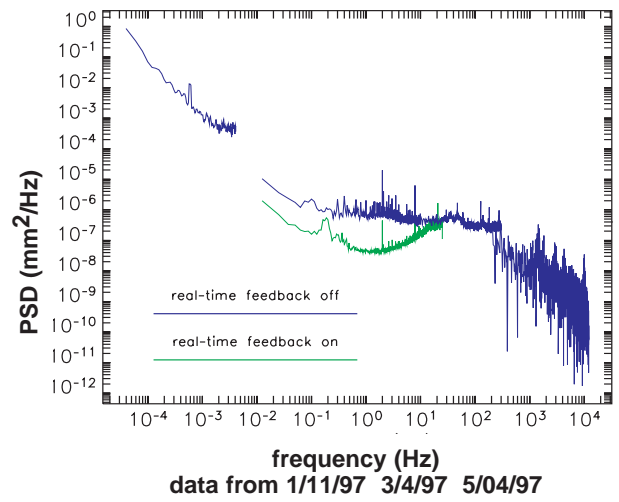


Fig. 5: APS vertical beam-motion power spectral density at insertion device source points.

tional run number. This is plotted both with and without the real-time feedback system operating, with the specifications indicated.

LIMITATIONS AND PERFORMANCE UPGRADES

The rf BPM system at the APS is now entering a mature phase of operation in which the hardware is essentially understood and planning to improve performance has begun. The system was designed to have broad-band turn-by-turn measurement capability to facilitate commissioning (for which it functioned very well) and provide postmortem analyses for extremely fast beam loss events (for which it also has been very useful). A system of this type results in a certain set of operational constraints and types of systematic errors. The bunch pattern is of critical importance to the operation of such a system and, as is commonly known, this has unfortunately placed constraints on what bunch patterns can be used at the APS. Specifically, a $1\text{-}\mu\text{s}$ or greater dead-time in the fill pattern is needed to allow the rf front-end bandpass filters to “ring-down” to a level where they do not impact the measurement of bunches that follow. One ongoing effort is to redesign these filters to allow bunch (or cluster) spacing as close as 100 ns. It is understood what is required to achieve this, and prototype configurations are under test.

As mentioned earlier, the AC orbit feedback now operates up to ~ 30 Hz. Plans are in the works for additional processing power to effectively raise the sampling rate from 1 kHz up to 2 kHz. This will allow access to more BPM data while achieving a higher correction bandwidth. Ultimately the identification and elimination of noise sources greater than about 60 Hz will be our most effective strategy for very high frequencies, using the feedback system itself as a diagnostic.

Another major effort in progress uses narrow-band “switched-receiver” electronics attached to pickup electrodes mounted on the small-gap insertion device vacuum chambers. The idea here is to rapidly switch (~ 10 kHz) each of the four pickup electrodes in turn through a common narrow-band heterodyne receiver, thus eliminating systematic errors associated with attempting to match sets of receiver electronics. These are expected to have improved performance in terms of systematic effects for DC correction. A complete production set of these receivers, including all of the data acquisition hardware, is under test at an unused insertion device location, and components to instrument all existing insertion devices are on order. These receivers will have their own set of systematic effects requiring study to achieve true submicron stability. This effort is already under way.

Nothing has been said thus far about the x-ray beam position monitors (X-BPMs). These are presently used for initial beamline steering and occasional adjustments, but otherwise are not presently active in DC or AC orbit correction. For the insertion device X-BPMs, this is a consequence of systematic errors resulting from multiple sources of unwanted stray radiation striking the photoemission-sensitive X-BPM blades. This manifests itself as a “gap-dependent offset”; i.e., as the insertion device gap is changed, the relative proportion of insertion device radiation to stray radiation changes, resulting in an apparent shift in beam position. Serious efforts are under way to study methods that will reduce or eliminate these stray radiation sources. One method being studied is a small realignment of accelerator and front-end components that would redirect the majority of stray radiation away from the X-BPMs.

During studies periods, local vertical DC correction capability has been demonstrated on bending magnet beamlines using X-BPMs. These X-BPMs, which are active in the vertical plane only, do not exhibit problems with systematic errors and are the most accurate means of determining long-term vertical beam drift. They are generally used as a benchmark against which our efforts at DC beam stabilization are measured.

Implementation strategies to combine local and global DC orbit correction utilizing X-BPMs are

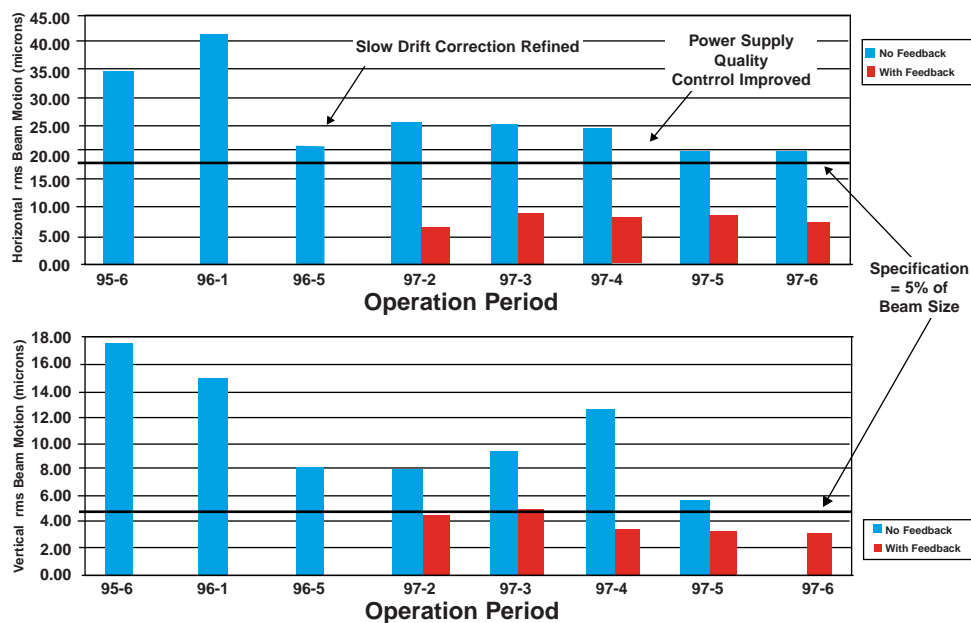


FIG. 6. APS beam stability history, 1995-present.

under investigation. Interface hardware is in place that provides all available X-BPM data to the real-time feedback system. Incorporation of this information into real-time orbit correction is proceeding in concert with efforts to understand X-BPM systematic effects and different correction algorithms.

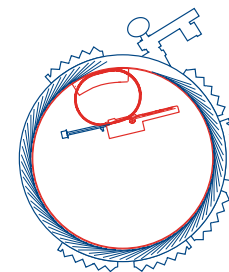
SUMMARY

Particle beam position measurement and correction at the Advanced Photon Source are presently at the state-of-the-art for synchrotron light sources, with few-micron stability now being accomplished routinely. Upgrade efforts on the rf BPMs, the X-BPMs, and new correction algorithms provide the promise of true submicron beam stabilization in the near future. ○

REFERENCES

- 1 Y. Chung, E. Kahana, “Performance of the Beam Position Monitor for the Advanced Photon Source,” Proceedings of SRI’95, Rev. Sci. Instrum. **66** (9), September 1995 (CD-ROM).
- 2 L. Emery, “Advancements in Orbit Drift Correction in the Advanced Photon Source Storage Ring,” Proceedings of PAC’97 (to be published).
- 3 A. Ropert, ESRF, Private Communication.
- 4 J. Carwardine and F. Lenkszus, “Architecture of the APS Real-Time Orbit Feedback System,” Proceedings of ICALEPCS’97 (to be published).
- 5 G. Decker, “Performance of the Advanced Photon Source,” Proceedings of PAC’97 (to be published).

BEAM ACCELERATION & STORAGE AT THE ADVANCED PHOTON SOURCE — OPERATIONS REPORT



Rod Gerig *Accelerator Systems Division, Argonne National Laboratory*

During fiscal year (FY) 1997, while many Advanced Photon Source (APS) beamlines were being commissioned, the Accelerator Systems Division focused attention on the goals of providing stable, reproducible beam positions; making the beam available for the users 90% of the scheduled time; and reducing the number of fills lost to faults to 1 every 24 hours. Steady and significant progress was made throughout the year, and, during the last three weeks of the final run of FY 1997, all goals were met. This level of operation has been surpassed throughout the first five months of FY 1998.

On October 1, 1997, the APS completed its first fiscal year of providing beam to users. This was also a period in which commissioning of accelerator systems continued and many accelerator improvements were made. Slow-orbit feedback, intended to maintain beam positions below the 1-Hz rate, received considerable attention early in the year. Real-time feedback, which maintains beam stability in the 1- to 30-Hz range, was inaugurated and became part of normal operations by the end of the year. The problems that led to lost storage ring "fills" were vigorously addressed, and by the end of the last run of the year, the APS was meeting goals established for the year.

Operational statistics were first kept in the final quarter of FY 1996. Goals were established in three main areas: beam stability, beam availability, and reliability. Table 1 shows the scheduled hrs, availability, and reliability in FY 1997 and FY 1998 to date.

BEAM AVAILABILITY

"Availability" is defined as the percentage of scheduled time that beam is supplied for user operations. The time it takes to refill the accelerator is regarded as "unavailability." The established goal was

90%. During FY 1997, 3141 hrs were scheduled. X-ray beam was available for 2450 hrs. Of the 691 hrs of unavailability (downtime), two categories of incidents accounted for most of the downtime: a small number of long interruptions and a large number of short interruptions (Fig. 1). In the first category, four incidents accrued 184 hrs, or 27%, of the year's downtime. In December 1996, operation was interrupted for 65 hrs when a studies period was invoked to improve orbit stability and reproducibility. This effort resulted in improved control of beam positions, as discussed below. In April 1997, two transformers failed in the booster dipole power supplies and accelerator operation was again interrupted for 65 hrs while the transformers were repaired. Interlocks have been added to this power supply to prevent a future occurrence. Other long-duration downtimes resulted from a linac waveguide problem and a lightning strike.

At the other extreme, the APS dealt with numerous short interruptions. With 473 fills during the year and an average refill time of about 40 minutes, a total of 315 hrs were spent filling the storage ring. This number does not include the time to repair any problems that may have caused the lost fills.

TABLE 1. X-ray availability in the APS storage ring.

	Scheduled User Hrs	X-ray Availability (hrs)	X-ray Availability %	Average Fill Duration without a Fault (MTBF, hrs)
1st Quarter FY 1997	518.6	370.7	71.5	5.1
2nd Quarter FY 1997	579.6	442.2	76.3	4.3
3rd Quarter FY 1997	812.7	584.7	71.9	5.6
4th Quarter FY 1997	1229.9	1052.2	85.6	10.4
FY 1997 Total	3140.8	2449.8	78.0	6.4
1st Quarter FY 1998	741.9	698.2	94.1	41.1
2nd Quarter FY 1998 (thru Feb.)	703.1	640.6	91.1	30.5
FY 1998 to Date (thru Feb.)	1444.9	1338.8	92.7	35.23

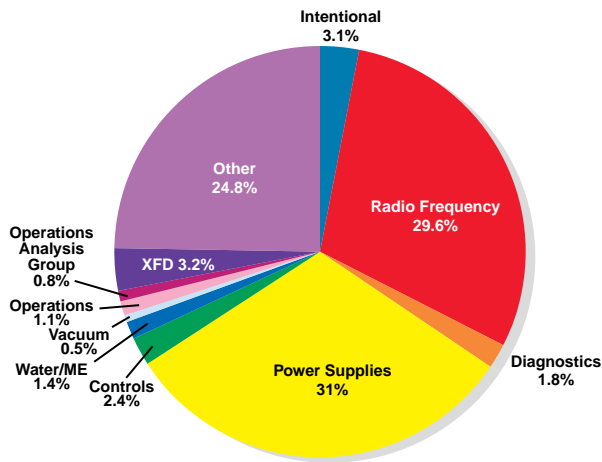


FIG. 1. Causes of FY 1997 downtime.

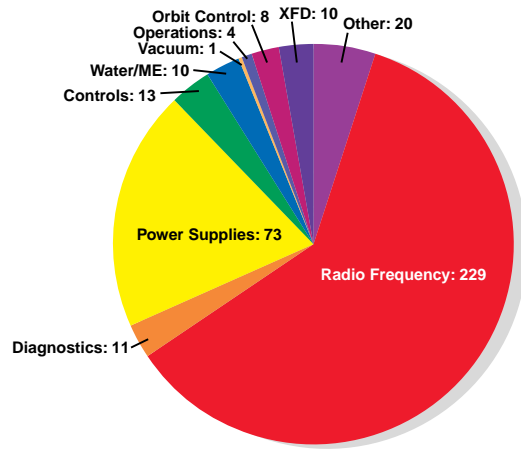


FIG. 2. FY 1997 reliability (number of faults).

In the first five months of FY 1998, 1444.9 hrs were scheduled, and x-ray beams were available 1338.8 hrs (92.7%).

BEAM RELIABILITY

Reliability is measured in terms of mean time between faults (MTBF), i.e., the amount of time that beam is delivered without a fault terminating a fill. The established goal was 24 hrs. Of the 473 fills during FY 1997, 379 (80%) were lost to faults. The majority of these (229) were caused by problems with the storage ring radio-frequency (rf) systems, as shown in Fig. 2. Intense effort was focused on eliminating these faults. Numerous improvements were made and problems solved. Most of the trips over the course of the year were inadvertent trips of the rf high-voltage protection circuit (crowbar). The final reoccurring problem was fixed in early September 1997; subsequently, the rf systems operated through the end of the run (~400 hrs) without a fault. Thus far in FY 1998, rf systems have led to 12 faults, 1 every 100 hrs.

The second largest cause of lost fills (73) was the storage ring power supply system. Several types of problems were discovered and rectified. The complexity of this system was amplified by the commissioning of the real-time feedback system. When real-time feedback is "on," power supplies are sent commands at a higher than normal rate, resulting in an increased probability of communications errors. By year's end, all of the outstanding power supply problems had been identified, and corrective actions were in many cases complete. Eight power supply faults occurred in FY 1998, 1 every 181 hrs.

In the first five months of FY 1998, only 38 faults have occurred for an MTBF of 35.2 hrs.

BEAM POSITION STABILITY/REPRODUCIBILITY

Considerable effort was spent during FY 1997 on achieving high-quality beam stability. Three dif-

ferent problems were encountered, each of which demanded different approaches in order to achieve the goals. These three problems were:

- Fill-to-fill reproducibility
- Precise closure of local bumps (i.e., steering displacement) so that when beam is steered for one user, it does not move for others
- Beam stability over a broad range of frequencies while beam is stored

Technical aspects of these topics and stability goals are discussed on pg. 25. Here, reliability concerns are addressed.

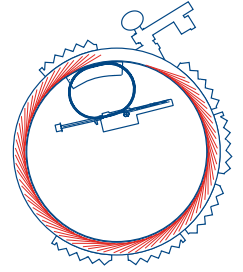
As commissioning of the APS continued and feedback algorithms were developed and implemented, it became clear that the beam position, as seen by the users, was not reproducible from fill to fill and, in fact, often changed during the course of a fill as the beam current dropped. This occurred in spite of stable, reproducible readbacks from the rf beam position monitors (BPMs), which are used in the feedback algorithms. It was realized that the rf BPMs are sensitive to both the distribution of bunches in the ring and the current. Compensation is now provided to correct for current dependency errors. Other efforts involved developing the correction algorithm to make it more robust in the presence of single BPM errors and identifying the sources of noise.

The second problem was addressed by modifying the software used in making the local bumps. Data from BPMs around the ring are used during correction with the constraint that the beam does what is expected in the bump region and does not move elsewhere.

The result of this work, much of which took place during an unscheduled interruption to user operations, has been a highly reproducible orbit from fill to fill and stable beam positions during the course of fills. ○

EXPERIMENTAL FACILITIES OPERATIONS & CURRENT STATUS

Antanas Raugas *Experimental Facilities Division, Argonne National Laboratory*



An Advanced Photon Source (APS) experiment (user) beamline consists of four functional sections: The x-ray beam source, either an insertion device (ID) or bending magnet (BM); the beamline front end (FE) section; hard x-ray optical elements; and the experiment or research stations. (For a more detailed explication of these components, see "The Advanced Photon Source Facility: A Brief Overview" on page 2.) The APS provides, operates, and maintains the x-ray sources and FEs for each sector. Beamline components are the responsibility of each Collaborative Access Team (CAT), which designs, builds, and operates the beamlines in its sector(s) with funds independently obtained from various sources. Each beamline constructed by the CATs is unique and supports the scientific program planned by a particular CAT.

At 7:13 a.m. on Sunday, March 26, 1995, the first x-rays from a BM radiation source in the APS storage ring (SR) were delivered down the Sector 1 BM beamline (1-BM) and into the 1-BM-A first optics enclosure (FOE) on the experiment hall floor. This milestone took place not only during the centennial of Wilhelm Röntgen's discovery of the x-ray, but also within one day of the 150th anniversary of his birth.

During July and early August of 1995, the first ID vacuum chamber and an undulator ID were installed in Sector 1 of the SR. The vacuum chamber was an initial-phase chamber with a vertical aperture of 12 mm and a minimum possible undulator gap of 14.5 mm. On August 9, 1995, with 7-GeV beam circulating in the storage ring, the photon shutters in the ID beamline FE were opened, and the first x-ray beams from an APS undulator were delivered to an FOE, where they were observed on a fluorescent screen.

After measuring the shielding integrity of the station, the initial experiments looked at the effect of an undulator on a stored 1-mA particle beam. Measurements of the closed-orbit distortion showed that the performance of the undulator exceeded specifications, evidence that undulator fabrication and magnetic tuning had met magnetic-field tolerances. The particle-beam emittance in the x and y direction was measured by imaging the source using zone plates. Results agreed with the design values for the emittance.

As of this writing, all of the FEs for the planned 20 sectors (40 beamlines) have been installed. Vacuum chambers for all of the IDs are also in place. The undulator chambers have a vertical aperture of 8 mm and a minimum possible gap of 10.5 mm. All of the IDs and FEs are functioning as expected with few failures. These systems have caused 22 hours of lost beam out of over 3100 hours scheduled to the user program during FY97.

User beamlines are in various stages of installation, commissioning, or operation. Twenty-five of the 40 currently committed APS user beamlines (16 ID and 9 BM) have transported x-ray beams to 66 research stations for a variety of experiments (Table 1). An additional 14 experiment stations on operating beamlines are undergoing construction or commissioning. Twenty other experiment stations on 3 new undulator beamlines and 5 new BM beamlines are being constructed. A summary of this data is shown in Fig. 1. Additional stations will continue to be constructed on the existing beamlines as the scope of these research programs expands. ○

TABLE 1. Dates of first commissioning of APS beamlines.

BEAMLINE	DATE OF FIRST BEAM
1-BM	03/26/95
1-ID	08/09/95
2-BM	06/24/96
2-ID	03/26/96
3-ID	01/24/96
5-BM	03/27/96
5-ID	05/22/96
7-BM	11/11/97
7-ID	08/16/96
8-ID	08/17/96
10-ID	08/08/96
11-ID	01/14/97
12-BM	03/26/96
12-ID	05/20/96
13-BM	09/17/96
13-ID	09/27/96
14-BM	04/21/97
14-ID	04/22/97
17-BM	10/14/96
17-ID	07/05/96
18-ID	06/12/97
19-BM	06/25/96
19-ID	03/26/96
20-ID	12/18/96
33-ID	07/03/96

SECTOR	CAT	ID VACUUM CHAMBER		FRONT-END		EXPERIMENT STATIONS									
		∅X Length	ID U/W-Period	BM	ID	BM					ID				
						A	B	C	D	E	A	B	C	D	E
1	SRI	8mm X 5m	U-33mm												
2	SRI	8mm X 5m	U-33mm												
3	SRI	5mm X 5m	U-27mm												
4															
5	DND	8mm X 5m	U-33mm												
6	MU	8mm X 5m	None												
7	MHATT	8mm X 5m	U-33mm												
8	IMM	8mm X 5m	U-33mm												
9	CMC	8mm X 5m	U-33mm												
10	MR	8mm X 5m	U-33mm												
11	BESSRC	SPECIAL	EMW												
12	BESSRC	8mm X 5m	U-33mm												
13	GEOCARS	8mm X 5m	U-33mm												
14	BIOCARS	12mm X 2.5m	W-85mm												
15	CHEMCARS	8mm X 5m	U-33mm												
16															
17	IMCA	8mm X 5m	U-33mm												
18	BIO	8mm X 5m	U-33mm												
19	SBC	8mm X 5m	U-33mm												
20	PNC	8mm X 5m	U-33mm												
33	UNI-1	8mm X 5m	U-33mm												
34	UNI-2	8mm X 2.5m	U-33mm												

Commissioned
 Being Commissioned
 Ready for Commissioning
 Being Installed
 Planned

FIG. 1. APS Collaborative Access Team beamline status — January 1998.

RECENT PUBLICATIONS

ACCELERATOR TECHNOLOGY

D. Barr and Y. Chung, "Hardware Design and Implementation of the Closed Orbit Feedback System at APS," Beam Instrumentation Workshop '96, Argonne, IL, May 6-9, 1996, AIP Conf. Proc. No. 390, pp. 368-374, March 1997.

W. Berg, B. Yang, A. Lumpkin, and J. Jones, "Design and Commissioning of the Photon Monitors and Optical Transport Lines for the APS Positron Accumulator Ring," Beam Instrumentation Workshop '96, Argonne, IL, May 6-9, 1996, AIP Conf. Proc. No. 390, pp. 483-490, March 1997.

M. Borland, "Doing Accelerator Physics Using SDDS, UNIX, and EPICS," Proc. of the International Conference on Accelerator and Large Experimental Physics Control Systems, ICALEPCS '95, Chicago, IL, October 30-November 3, 1995, pp. 382-391, January 1997.

M. Borland, "The Self-Describing Data Sets File Protocol and Toolkit," Proc. of the International Conference on Accelerator and Large Experimental Physics Control Systems, ICALEPCS '95, Chicago, IL, October 30-November 3, 1995, pp. 653-662, January 1997.

J. Carwardine, "An Introduction to Plant Monitoring through the EPICS Control System," Proc. of the International Conference on Accelerator and Large Experimental Physics Control Systems, ICALEPCS '95, Chicago, IL, October 30-November 3, 1995, pp. 489-496, January 1997.

Y. Chung, D. Barr, G. Decker, J. Galayda, F. Lenkszus, A. Lumpkin, and A. J. Votaw, "Digital Closed Orbit Feedback System for the Advanced Photon Source Storage Ring," Proc. of the International Conference on Accelerator and Large Experimental Physics Control Systems, ICALEPCS '95, Chicago, IL, October 30-November 3, 1995, pp. 263-268, January 1997.

D. J. Ciarlette and R. Gerig, "Operational Experience from a Large EPICS-Based Accelerator Facility," Proc. of the International Conference on Accelerator and Large Experimental Physics Control Systems, ICALEPCS '95, Chicago, IL, October 30-November 3, 1995, pp. 322-327, January 1997.

K. Evans, Jr., "Simulating Using Xorbit with EPICS," Proc. of the International Conference on Accelerator and Large Experimental Physics Control Systems, ICALEPCS '95, Chicago, IL, October 30-November 3, 1995, pp. 756-762, January 1997.

R. Fuja, N. Arnold, W. Berg, G. Decker, R. Dortwegt, M. Ferguson, N. Friedman, J. Gagliano, A. Lumpkin, G. Nawrocki, and X. Wang, "The APS Machine Protection System (MPS)," Beam Instrumentation Workshop '96, Argonne, IL, May 6-9, 1996, AIP Conf. Proc. No. 390, pp. 454-459, March 1997.

E. Kahana and Y. Chung, "Commissioning Results of the APS Storage Ring RF Beam Position Monitors," Beam Instrumentation Workshop '96, May 6-9, 1996, AIP Conf. Proc. No. 390, pp. 266-272, March 1997.

J. Kirchman, "Experimental Results of the Design for the APS PID Global Orbit Control System," Proc. of the International Conference on Accelerator and Large Experimental Physics Control Systems, ICALEPCS '95, Chicago, IL, October 30-November 3, 1995, January 1997.

M. Knott, "Communications in Support of Software Sharing and Collaborative Development," Proc. of the International Conference on Accelerator and Large Experimental Physics Control Systems, ICALEPCS '95, Chicago, IL, October 30-November 3, 1995, pp. 370-375, January 1997.

J. Kowalkowski, "A Cost Effective Way to Operate Instrumentation Using the Motorola MVME162 Industry Pack Bus and HiDEOS," Proc. of the International Conference on Accelerator and Large Experimental Physics Control Systems, ICALEPCS '95, Chicago, IL, October 30-November 3, 1995, pp. 1022-1026, January 1997.

J. Kowalkowski, "An Object-Oriented Approach to Low-Level Instrumentation Control and Support," Proc. of the International Conference on Accelerator and Large Experimental Physics Control Systems, ICALEPCS '95, Chicago, IL, October 30-November 3, 1995, pp. 113-120, January 1997.

D. Leibfritz, "Administering Network Information for PCs," Sys Admin: The Journal for UNIX Systems Administrators 6 (1), 74-79, January 1997.

F. Lenkszus and R. Laird, "The Advanced Photon Source Event System," Proc. of the International Conference on Accelerator and Large Experimental Physics Control Systems, ICALEPCS '95, Chicago, IL, October 30-November 3, 1995, pp. 345-350, January 1997.

- F. Lenkszus and R. Laird, "The Advanced Photon Source Injection Timing System," Proc. of the International Conference on Accelerator and Large Experimental Physics Control Systems, ICALEPCS '95, Chicago, IL, October 30-November 3, 1995, pp. 567-571, January 1997.
- E. Lessner and K. Symon, "A Tracking Code for Injection and Acceleration Studies in Synchrotrons," 1996 Computational Accelerator Physics Conference, Williamsburg, VA, September 24-27, 1996, AIP Conf. Proc. No. 391, pp. 185-190 (1997).
- A. Lumpkin, "Commissioning Results of the APS Storage Ring Diagnostics Systems," Beam Instrumentation Workshop '96, Argonne, IL, May 6-9, 1996, AIP Conf. Proc. No. 390, pp. 152-172, March 1997.
- A. H. Lumpkin, "Observations of Bunch Lengthening Effects in the APS 7-GeV Storage Ring," Free Electron Laser Conference '96, Rome, Italy, August 26-31, 1996, Nucl. Instrum. Meth. in Phys. Res. A 393, 50-54 (1997).
- A. H. Lumpkin, "On the Path to the Next Generation of Light Sources," Free Electron Laser Conference '96, Rome, Italy, August 26-31, 1996, Nucl. Instrum. Meth. in Phys. Res. A 393, 170-177 (1997).
- Q. Ma, R. Rosenberg, C. Kim, J. Grepstad, and P. Pianetta, "Microscopic chemical state identification of a silicon-carbide fiber by soft x-ray photoabsorption spectroscopy," Appl. Phys. Lett. 70 (18), 2389-2391, (1997).
- Q. Ma, R. A. Rosenberg, C. Kim, J. Grepstad, P. Pianetta, T. Droubay, D. Dunham, and B. Tonner, "Comparative magnetic-field imaging, electric-field imaging, and scanning auger microscopy study of metal-matrix composites," J. Elect. Spectrosc. and Rel. Phenom. 84, 99-107 (1997).
- G. Nawrocki, "Monitoring Commercial Conventional Facilities Control with the APS Control System - The Metasys-to-EPICS Interface," Proc. of the International Conference on Accelerator and Large Experimental Physics Control Systems, ICALEPCS '95, Chicago, IL, October 30-November 3, 1995, pp. 598-601, January 1997.
- D. Patterson, "Initial Commissioning Results from the APS Loss Monitor System," Beam Instrumentation Workshop '96, May 6-9, 1996, AIP Conf. Proc. No. 390, pp. 460-467, March 1997.
- R. Rosenberg, Q. Ma, W. Farrell, M. Keefe, and D. C. Mancini, "X-ray welding of metal-matrix composites," Rev. Sci. Instrum. 68 (6), 2550-2553 (1997).
- N. S. Sereno and R. Fuja, "Positron Beam Position Measurement for a Beam Containing Both Positrons and Electrons," Beam Instrumentation Workshop '96, Argonne, IL, May 6-9, 1996, AIP Conf. Proc. No. 390, pp. 316-323, March 1997.
- K. Sidorowicz, "The APS Control System Network," Proc. of the International Conference on Accelerator and Large Experimental Physics Control Systems, ICALEPCS '95, Chicago, IL, October 30-November 3, 1995, pp. 68-72, January 1997.
- K. R. Symon, "Derivation of Hamiltonians for Accelerators," APS Technical Bulletin ANL/APS/TB-28, September 1997.
- L. C. Teng, "Synchrotron Radiation Sources and Research," Proc. of the First International Conference on Frontiers of Physics, Shantou, China, August 5-9, 1995, pp. 718-733, L-F. Li, K. K. Phua, S. S. M. Wong, B-L. Young (Eds.), World Scientific (1997).
- M. M. White and E. S. Lessner, "The advanced photon source (APS) linear accelerator as a source of slow positrons," Appl. Surf. Sci. 116, 87-90 (1997).
- B. Yang and A. H. Lumpkin, "Particle-Beam Profiling Techniques on the APS Storage Ring," Beam Instrumentation Workshop '96, Argonne, IL, May 6-9, 1996, AIP Conf. Proc. No. 390, pp. 491-497, March 1997.

EXPERIMENTAL RESULTS & BEAMLINE TECHNOLOGY

- M. Agamalian, J. M. Drake, S. K. Sinha, and J. Axe, "Neutron Diffraction Study of the Pore Surface Layer of Vycor Glass," Phys. Rev. E 55 3021-3027 (1997).
- I. Basdogan, T. J. Royston, J. Barraza, D. Shu, and T. M. Kuzay, "A Theoretical and Experimental Study of the Vibratory Behavior of a High-Precision Optical Positioning Table," Proc. of DETC'97, 1997 ASME Design Engineering Technical Conferences, DETC97/VIB-4215 1-11 (1997).
- I. Basdogan, T. J. Royston, A. A. Shabana, J. Barraza, D. Shu, and T. M. Kuzay, "Analysis of High-Precision Optical Positioning Systems for Vibration Stability at the Advanced Photon Source," SPIE Vol. 3132 47-55 (1997).
- P. B. Fernandez, T. Graber, W.-K. Lee, D. M. Mills, C. S. Rogers, and L. A. Assoufid, "Test of a High-Heat-Load Double-Crystal Diamond Monochromator at the Advanced Photon Source," Nucl. Instrum. Meth. Phys. Res. A 400 476-483 (1997).

- B. Fultz, C. C. Ahn, E. E. Alp, W. Sturhahn, and T. S. Toellner, "Phonons in Nanocrystalline 57Fe," *Phys. Rev. Lett.* **79**, 937-940 (1997).
- M. Hoffberg, R. Laird, F. Lenkzsus, C. Liu, B. Rodricks, and A. Gelbart, "The Development of a High-Speed 100 fps CCD Camera," *Nucl. Instrum. Meth. Phys. Res. A* **392**, 214-219 (1997).
- A. Khounsary, W. Yun, E. Trakhtenberg, S. Xu, L. Assoufid, and W. K. Lee, "Contact-Cooled U-Monochromator for High Heat Load X-ray Beamlines," *SPIE High Heat Flux Eng. Conf. Proc.* (1996).
- V. I. Kushnir, P. M. Abbamonte, A. T. Macrander, and M. Schwoerer-Böhning, "Backscattering Channel-Cut High Resolution Monochromator for Inelastic X-ray Scattering," *Proc. of SPIE* **3151**, 324-328 (1997).
- H.-R. Lee, "A Novel Iterative Optimizing Quantization Technique for Limited Data Computed Tomography," *Optical Engineering Monthly Journal*, April 1997.
- W.-K. Lee, P. B. Fernandez, A. Khounsary, W. Yun, and E. Trakhtenberg, "Advanced Photon Source Undulator Beamline Tests of a Contact-Cooled Silicon U-Shaped Monochromator," *Proc. of SPIE* **3151**, 208-215 (1997).
- C. Liu, D. Shu, T. M. Kuzay, R. Wen, and C. A. Melendres, "Ion Beam Induced Surface Modification of Chemical Vapor Deposition Diamond for X-ray Beam Position Monitor Applications," *J. Vac. Sci. Technol. A* **15**, 1200-1205 (1997).
- A. T. Macrander, M. Schwoerer-Böhning, P. M. Abbamonte, and M. Hu, "High Resolution Monochromator for Inelastic Scattering Studies of High Energy Phonons Using Undulator Radiation at the Advanced Photon Source," *Proc. of SPIE* **3151**, 271-281 (1997).
- D. M. Mills, "X-ray Optics Developments at the APS for the Third Generation of High-Energy Synchrotron Radiation Sources," *J. Synchrotron Rad.* **4**, 117-124 (1997).
- S. G. J. Mochrie, A. M. Mayes, A. R. Sandy, M. Sutton, S. Brauer, G. B. Stephenson, D. L. Abernathy, and G. Grubel, "Dynamics of Block Copolymer Micelles Revealed by X-ray Intensity Fluctuation Spectroscopy," *Phys. Rev. Lett.* **78**, 1275-1278 (1997).
- P. H. Mui, G. Srajer, and D. M. Mills, "In-situ Surface Monitoring System for Synchrotron Mirrors under High Heat Load," *Applied Optics* **36**, 5546-5551 (1997).
- M. Pisharody, P. K. Job, S. Magill, J. Proudfoot, and R. Stanek, "Measurement of Gas Bremsstrahlung from Electron Storage Rings," *Nucl. Instrum. Meth. Phys. Res. A* **401**, 442-462 (1997).
- K. J. Randall, J. Z. Xu, D. Graessle, J. J. Fitch, S. DiFonzo, B. R. Mueller, and W. Jark, "Reflectivity Measurements of Multilayer Optics for Use on the Advanced Photon Source Soft X-ray Beamlines," *NLSL Annual Report* (1996).
- M. Sanchez del Rio and R. J. Dejus, "XOP: A Multiplatform Graphical User Interface for Synchrotron Radiation Spectral and Optics Calculations," *Proc. of SPIE* **3152**, 148-157 (1997).
- M. Schwoerer-Böhning, P. M. Abbamonte, A. T. Macrander, and V. I. Kushnir, "A Spherical Bent Focusing Analyzer for High Resolution Inelastic X-ray Scattering," *Proc. of SPIE* **3151**, 282-286 (1997).
- S. K. Sinha, Y. P. Feng, C. A. Melendres, D. D. Lee, T. P. Russell, S. K. Satija, E. B. Sirota, and M. K. Sanyal, "Off-Specular X-ray Scattering Studies of the Morphology of Thin Films," *Physica A* **231**, 99-110 (1996).
- R. K. Smither, A. M. Khounsary, and S. Xu, "Potential of a Beryllium X-ray Lens," *Proc. of SPIE* **3151**, 150-163 (1997).
- S. J. Stein, "Personnel Safety System Status Reporting via EPICS at the Advanced Photon Source," *Proc. of the 1995 International Conference on Accelerator and Large Experimental Physics Control Systems (ICALPECS '95)*, Oct. 29 - Nov. 3, 1995, Chicago, IL, eds. M. Crowley-Millings, P. Lucas, and P. Schoessow, *Fermilab Report CONF-96/069*, 615-619.
- S. J. Stein, C. L. Seaver, G. J. Nawrocki, and M. R. Kraimer, "Data Exchange from Allen-Bradley PLC-Based Systems to EPICS at the Advanced Photon Source," *Proc. of the 1995 International Conference on Accelerator and Large Experimental Physics Control Systems (ICALPECS '95)*, Oct. 29 - Nov. 3, 1995, Chicago, IL, eds. M. Crowley-Millings, P. Lucas, and P. Schoessow, *Fermilab Report CONF-96/069*, p. 20-624.
- T. S. Toellner, M. Y. Hu, W. Sturhahn, K. Quast, and E. E. Alp, "Inelastic Nuclear Resonant Scattering with Sub-meV Energy Resolution," *Applied Physics Letters* **71**, 2112-2114 (1997).
- P. von Ballmoos, A. Kohnle, J. F. Olive, G. Vedrenne, R. K. Smither, P. B. Fernandez, and T. Graber, "A Tunable Crystal Diffraction Telescope for the International Space Station," *ESA Symposium Proceedings on "Space Station Utilization"* (SP-385, December 1996) pp. 433-437.

INFORMATION SOURCES

ADVANCED PHOTON SOURCE RESEARCH WELCOMES SUBMISSION OF ARTICLES ON RELEVANT TOPICS.

ADDRESS CORRESPONDENCE & REQUESTS FOR ADDITIONAL INFORMATION ON SUBJECTS IN THIS ISSUE TO:

Advanced Photon Source Research

Bldg. 401, Rm A4119

Argonne National Laboratory

9700 S. Cass Ave.

Argonne, IL 60439 U.S.A.

or fenner@aps.anl.gov

Also: Write to the address above for a copy of *The Advanced Photon Source - A National Synchrotron Radiation Research Facility (ANL/APS/TB-25-Rev.)*.

FOR INFORMATION ON THE APS USER PROGRAM, CONTACT THE:

User Administration Office

Advanced Photon Source

Bldg. 401. Rm. B1154A

Argonne National Laboratory

9700 S. Cass Ave.

Argonne, IL 60439 U.S.A.

630.252.5981

or barr@aps.anl.gov

FOR INQUIRIES ABOUT OTHER ARGONNE NATIONAL LABORATORY RESEARCH PROGRAMS, WRITE TO:

Office of Public Affairs

Bldg. 201

Argonne National Laboratory

9700 S. Cass Ave.

Argonne, IL 60439 U.S.A.

THE ADVANCED PHOTON SOURCE WORLD WIDE WEB SITE IS AT:

<http://www.aps.anl.gov/welcome.html>

THE ADVANCED PHOTON SOURCE USER ADMINISTRATION OFFICE WORLD WIDE WEB PAGE IS AT:

<http://www.aps.anl.gov/xfd/communicator/useroffice/ui>

A WEB-BASED OVERVIEW OF THE ADVANCED PHOTON SOURCE CAN BE ACCESSED AT:

<http://www.aps.anl.gov/overview/ovrvu/frnt/welcome.frntpg1.html>

THE ARGONNE NATIONAL LABORATORY WORLD WIDE WEB SITE IS AT:

<http://www.anl.gov/>

THE UNIVERSITY OF CHICAGO'S WORLD WIDE WEB SITE IS AT:

<http://www.uchicago.edu/>

THE U.S. DEPARTMENT OF ENERGY'S WORLD WIDE WEB SITE IS AT:

<http://www.er.doe.gov/>

ADVANCED PHOTON SOURCE RESEARCH IS PUBLISHED AT ARGONNE NATIONAL LABORATORY-EAST, ARGONNE, ILLINOIS

EDITORIAL STAFF:

Richard B. Fenner

Catherine E. Eyberger

Susan M. Picologlou

DESIGN:

RBF

PHOTOGRAPHY:

Argonne National Laboratory Photography Group (unless otherwise noted)

DATA: THE APS USER PROGRAM

Sectors 1, 2, and 3 - Synchrotron Radiation Instrumentation Collaborative Access Team (SRI-CAT):

Development of high-heat-load and other unique x-ray optical components, insertion devices, and beam diagnostics.

Development of innovative synchrotron-radiation-based techniques for all areas of basic and applied science. These techniques include generation and use of polarized x-rays, high-energy x-ray scattering, soft and hard x-ray microprobes, x-ray imaging, use and application of coherent x-rays, deep x-ray lithography, inelastic x-ray scattering, and nuclear resonant scattering.

Sector 5 - E.I. DuPont de Nemours and Co.-Northwestern University-The Dow Chemical Co. (DND) CAT: Materials science and engineering, esp. the study of two-dimensional and quasi-two-dimensional atomic structures (surfaces, interfaces, and thin films) incl. solid-liquid electrolyte interfaces, oxide surfaces, intercrystalline interfaces, thin-film growth *in situ*, and polymer film surfaces. In polymer science and technology: polymer deformation, crystallization and melting of polymers, and polymer de-formation and fracture. Also atomic structure of bulk materials.

Sector 6 - Midwest Universities (μ) CAT: Magnetic x-ray scattering (magnetic structures and phase transitions); surface and interface scattering (kinetics and growth of two-dimensional systems, the role of defects in epitaxy, ordered nonepitaxial overlayers, and phase transitions in liquid crystals); microdiffraction (small-grained samples of unusual interest, i.e., quasicrystals and mineral particles of extraterrestrial origin); bulk and surface phase transitions.

Sector 7 - Center for Real-Time X-ray Studies (MHATT) CAT: Time-resolved studies of materials under real dynamic conditions: microscopic analysis of physical and chemical processing, behavior under stress and structural relaxation, and the kinetic mechanisms of growth; new kinds of coherent spectroscopic measurements of solids and complex fluids.

Sector 8 - MIT-McGill-IBM (IMM) CAT: Broad range of materials science, physics, and chemistry projects incl.: intensity fluctuation spectroscopy studies using coherent x-rays; SAXS and USAXS studies of polymers and complex fluids; scattering studies of surface phase transformations, incl. studies of phase transformation kinetics and studies of surface critical phenomena; x-ray scattering studies at very low temperatures, incl. studies of helium in a random aerogel matrix; x-ray magnetic scattering studies of novel magnetic systems, incl. disordered magnetic systems; studies of solid-electrolyte interfaces; and characterization of technologically important magnetic and polymer thin films and interfaces.

Sector 9 - Complex Materials Consortium (CMC) CAT: Structural characterization of complex materials, incl. complex fluids and self-assembling systems, surfaces and interfaces, and heterogeneous materials, using time-dependent diffraction and scattering studies, high-resolution small-angle scattering and crystallography, surface scattering, photon-correlation spectroscopy, magnetic scattering, and several types of imaging techniques.

Sector 10 - Materials Research (MR) CAT: X-ray scattering, reflectivity, DAFS, and XAFS for *in-situ* studies of complex materials, incl. structural phase changes (esp. in non-equilibrium systems), disordered systems (e.g., alloys, amorphous materials), growth and recrystallization processes at surfaces and interfaces, *in-situ* time-dependent studies of catalysts, polymers (e.g., dynamics of block co-polymers, single-fiber studies, etc.), the structure of static and dynamic confined liquids, and organic thin films and self-assembled systems.

Sectors 11 and 12 - Basic Energy Sciences Synchrotron Radiation Center (BESSRC) CAT: Materials science, chemical science, and atomic physics, incl. time-resolved studies of photo-excited states in photosynthetic materials, real-time investigations of chemical reactions, and time-dependent structural studies of phase transformations in solid compounds; structural studies of actinides, studies of ultra-small crystals; trace element analysis, surface and interface studies; high-energy x-ray scattering and magnetic Compton scattering to investigate material properties, circularly polarized x-rays for study of structural and magnetic properties of alloys and thin films.

Consortium for Advanced Radiation Sources (CARS)

Sector 13 - GeoCARS-CAT and SoilEnviroCARS-CAT,

Sector 14 - BioCARS-CAT,

Sector 15 - ChemMatCARS-CAT:

Structural biology: Emphasis on elucidation of molecular structure, esp. from crystals with very large unit cells, such as viruses, and from microcrystals and crystals suitable for multiple wavelength anomalous dispersion phasing; time-resolved studies of biological processes in crystals. Earth planetary, and soil and environmental sciences: Surface scattering, microcrystallography, and time-resolved work, as well as high-pressure diffraction, spectroscopy, microprobe analyses, and powder diffraction. Materials chemistry and materials science studies: Surface scattering of liquids and polymer surfaces, time-resolved small-angle and wide-angle x-ray scattering studies of polymers and other materials, and time-resolved and valence/element specific chemical crystallography.

Sector 17 - Industrial Macromolecular Crystallography Association (IMCA) CAT: Determine structures of biological macromolecules to aid in the design of biologically active compounds for medicine and agriculture, understand the mechanism of action of biological macromolecules, guide protein engineering to develop molecules with improved properties, assist in product development, and meet regulatory requirements.

Sector 18 - Biophysics (Bio) CAT: Study of the structure and dynamics of biological and related systems at the molecular level, with a focus on partially ordered samples such as membranes, fibers, and solutions, using resonant (anomalous) and nonresonant x-ray diffraction, and XAFS spectroscopy, with emphasis on time-resolved studies, polarized XAFS, hybrid diffraction/spectroscopic techniques, and novel techniques.

Sector 19 - Structural Biology Center (SBC) CAT: Macromolecular crystallography, incl. monochromatic data collection from microcrystals; monochromatic data collection from crystals with large cell dimensions; monochromatic data collection from large numbers of closely similar crystal structures; data collection at several discrete energies from a single crystal for use in MAD phasing; and polychromatic (Laue) data collection for static or kinetic structure analysis.

Sector 20 - Pacific Northwest Consortium (PNC) CAT: Environmental and materials sciences, using spatial and time-resolved XAFS and diffraction (incl. Laue diffraction), spatial resolved tomography, fluorescence microprobe analysis, surface and interface diffraction, x-ray Raman scattering, diffraction, anomalous fine structure, and macromolecular crystallography. Materials research includes fundamental studies and studies relating to the interaction of materials with the environment. Environmental sciences studies involving natural systems that are heterogeneous and complex. Macromolecular crystallography to investigate biological methods of sequestering environmental toxins in addition to basic studies.

Sector 33 - A University-National Laboratory-Industry (UNI) CAT: Physics, chemistry, biology, materials science, chemical engineering, and geology, with emphasis on projects that are cross-disciplinary in both scientific interest and methodology, using crystallography, diffuse x-ray scattering, surface-interface diffraction and scattering, millivolt/nanovolt-resolution scattering spectroscopy, magnetic x-ray scattering, ultra-small-angle scattering, time-resolved structural scattering, topography, imaging, and x-ray absorption spectroscopy.

Sector 34 - UNI-CAT: Dedicated microprobe and coherent x-ray diffraction beamline for study of structural dynamics on the critical "mesoscopic"-length-scales that determine the fundamental physics and dynamics of phase transformations and micro-structural evolution; coherent scattering for phase sensitive information on local structural fluctuations, with time correlation of coherent diffraction yielding direct information on structural dynamics from microns to Å. Focused microbeams of white and monochromatic x-rays, in connection with precision scanning techniques, to provide microscale chemical, structural, and structural dynamics information using scanning Bragg scattering, diffuse scattering, and fluorescence techniques.